

Article

Phenomenology of the Neutral-Ionic Valence Instability in Mixed Stack Charge-Transfer Crystals

Matteo Masino, Nicola Castagnetti and Alberto Girlando *

Dip. di Scienze Chimiche, della Vita e della Sostenibilità Ambientale and INSTM-UdR di Parma, Parco Area delle Scienze, Università di Parma, I-43124 Parma, Italy; matteo.masino@unipr.it (M.M.); nicola.castagnetti@studenti.unipr.it (N.C.)

* Correspondence: alberto.girlando@unipr.it; Tel.: +39-0521-905-443

Academic Editors: Anna Painelli, Helmut Cölfen and Alberto Girlando

Received: 15 March 2017; Accepted: 6 April 2017; Published: 11 April 2017

Abstract: Organic charge-transfer (CT) crystals constitute an important class of functional materials, characterized by the directional charge-transfer interaction between π -electron Donor (D) and Acceptor (A) molecules, with the formation of one-dimensional ...DADAD... stacks. Among the many different and often unique phenomena displayed by this class of crystals, Neutral-Ionic phase transition (NIT) occupies a special place, as it implies a *collective* electron transfer along the stack. The analysis of such a complex yet fascinating phenomenon has required many years of investigation, and still presents some open questions and challenges. We present an updated and extensive summary of the phenomenology of the temperature induced NIT, with emphasis on the spectroscopic signatures of the transition. A much shorter summary is given for the NIT induced by pressure. Finally, we report on the exploration, by chemical substitution, of the phase space of ...DADAD... CT crystals, aimed at finding materials with important semiconducting or ferroelectric properties, and at understanding the subtle factors determining the crystal packing.

Keywords: charge-transfer crystals; Neutral-Ionic phase transition; electron-phonon coupling; optical spectroscopy; valence and Peierls instability

1. Introduction

Organic charge-transfer (CT) crystals occupy a special place among functional molecular crystals. They are among the first examples of low-dimensional systems, since the strongly directional CT interaction between π -electron Donor (D) and Acceptor (A) molecules dominates over the other intermolecular interactions and yields the formation of one-dimensional stacks. Furthermore, the presence of low-lying CT excitation(s) gives rise to many different transport, optical and magnetic properties. These properties strongly depend on the molecular stacking/packing and on degree of charge-transfer or ionicity ρ from D to A. A main classification concerning stacking is in segregated stack CT crystals, where each stack is made up of only one type of molecule, either D or A, and in mixed stack (ms) CT crystals, where the chain is made up of both D and A molecules. For segregated stacks ρ changes from 0.5 to 1, i.e., the ground state is always ionic, whereas for ms stacks it changes from 0 to 1, with 0.5 phenomenologically separating neutral (N) and ionic (I) ground states [1].

The degree of CT depends on the balance between the cost of ionizing a DA pair $I_P - E_A$, (I_P is the D ionization potential, and E_A is the A electron affinity) and the Madelung energy M [2]. For ms crystals the crossover between N and I ground states occurs when $I_P - E_A \approx M$. J. B. Torrance realized that by increasing M through the application of pressure or temperature the N-I borderline could be experimentally crossed [3,4], giving rise to a new kind of phase transition, the Neutral-Ionic transition (NIT). Later on Koshihara et al. found that for systems close to NIT a light pulse may also induce the transition, populating a long-lived metastable state [5]. Interestingly enough, a valence

instability similar to NIT, implying a symmetry breaking already present in ms systems, can occur in segregated stack crystals, where it is called Charge Order (CO) transition [6].

NIT is a *collective* electron transfer from D to A, implying charge, spin and phonon degrees of freedom, and as such is a complex phenomenon, with many facets, whose analysis required many years of investigations. The aim of the present paper is to give an updated summary of the phenomenology of NIT, with emphasis on the experimental aspects. Previous summaries can be found in [7–9]. The paper will prioritize the work performed by our research group, also presenting some unpublished data from our laboratory.

We shall restrict the attention on the 1:1 ms CT crystals, where the stack is made by alternating D and A molecules. In addition, we shall not discuss light induced NIT and related phenomena: Strictly speaking, these are not true phase transitions, but transient phenomena related to a metastable domains. We shall instead consider all systems displaying a change of ionicity driven by the increase in Madelung energy, although in some cases the N-I borderline $\rho \simeq 0.5$ is not crossed. On the other hand, we remark that the N and I phases can be distinguished on a more fundamental basis than the ρ value: As it was early recognized, mixed stack CT crystals are also subject to the Peierls instability, yielding stack dimerization $\cdots DA DA DA \cdots$ [10]. Peierls dimerization, implying both electron and spin degrees of freedom (generalized Peierls) may occur at the same time as the ionicity change [10], or independently [11]. In fact, on the ionic side a regular stack is intrinsically unstable towards dimerization (degenerate ground state), whereas in the proximity of the N-I borderline ($\rho \geq 0.3$ – 0.4) the instability is conditional, i.e., depends on the strength of electron-lattice phonon coupling [12,13]. The competition between two instabilities, a first-order one driven by the 3D Madelung energy (valence instability, order parameter: ρ) and a second order one, driven by 1D electron-lattice phonon (e-ph) coupling (Peierls instability, order parameter: stack dimerization) is what makes NIT such a complex and intriguing phenomenon.

2. Temperature Induced NIT

Although pressure induced NIT has been discovered first [3], most of the subsequent investigations have focused on the temperature induced NIT, so we shall start from them. The number of CT crystals undergoing T -induced valence instabilities is very limited, the main features of the transitions being summarized in Table 1. We have excluded from the Table systems whose ionicity continuously increase by lowering T without crossing the N-I borderline, ionic systems only undergoing a Peierls transition without ionicity change [7], or systems undergoing quantum phase transitions [14].

Table 1. Temperature induced Neutral-Ionic transitions (ambient pressure).

System ^a	T_{NI}^b (K)	$\Delta\rho$ Jump	$\rho(T)$ Range	Ref.
TTF–CA	81–83	0.21	0.2–0.6	[10,15]
TTF–BrCl ₃ BQ	68	0.16	0.2–0.6	[16]
DMeTTF–CA	65	0.02	0.2–0.4	[17]
DMeTTF–BrCl ₃ BQ	54	0.1	0.2–0.6	[18]
DMeTTF–2,5Br ₂ Cl ₂ BQ	49	0.06	0.3–0.4	[18]
TMB–TCNQ	205–235	0.1	0.3–0.4	[19]
CIMePD–DCNQI	200 ^c	absent	0.3–0.6	[20]

^a TTF: tetrathiafulvalene; CA: chloranil; BrCl₃BQ: bromo-trichloro-*p*-benzoquinone; CIMePD: 2-chloro-5-methyl-*p*-phenylendiamine; DCNQI: 2,5-dimethyl-dicyanoquinonediimine; DMeTTF: 4,4'-dimethyl-TTF; 2,5Br₂Cl₂BQ: 2,5-dichloro-3,6-dibromo-*p*-benzoquinone; TMB: 3,3',5,5'-tetramethylbenzidine; TCNQ: tetracyanoquinodimethane. ^b When present, the T interval indicates hysteresis. ^c Temperature of N-I borderline crossing.

Table 1 shows that the number of systems undergoing temperature-induced NIT is extremely limited. Essentially, they can be divided in four different types: TTF–CA and TTF–BrCl₃BQ, which display a first order neutral-ionic transition (ρ changes from about 0.2 to 0.6 at T_c) accompanied

by stack dimerization, yielding a ferroelectric ground state. DMeTTF-CA, which has a transition at the borderline between first and second order, and the very similar, but less studied DMeTTF-2,5Br₂Cl₂BQ. TMB-TCNQ, which displays a first order transition with large hysteresis, accompanied by dimerization, but ending in a quasi-neutral ground state. Finally, CMePD-DMeDCNQI, unique continuous neutral-ionic phase transition, characterized by dipolar disorder and by the absence of long-range order in the dimerization.

In the following we shall examine in detail the phenomenology of the above four classes of systems, first making a direct comparison between the chemically similar and widely studied TTF-CA and DMeTTF-CA, then dealing separately with TMB-TCNQ and CMePD-DMeDCNQI.

2.1. TTF-CA and DMeTTF-CA

2.1.1. Valence Instability and Stack Dimerization

Vibrational spectroscopy, and infrared (IR) spectroscopy in particular, offers basic information on NIT. In fact, the ionicity can be estimated by looking at selected intra-molecular charge-sensitive vibrations, whose frequencies depend linearly on ρ [21,22]. In the case of ms crystals, however, totally symmetric modes cannot be used, as their frequency is perturbed by the interaction with the CT electron (electron-molecular vibration, e-mv, interaction) [21,23]. In the case of ms CT crystals involving chloranil, the b_{1u} ν_{10} C=O antisymmetric stretching is the most apt charge sensitive mode, in virtue of its large ionization frequency shift (160 cm⁻¹) and of its occurrence in a spectral interval (1685–1525 cm⁻¹) relatively free from interference from other vibrational modes [24].

Figure 1 reports the IR spectra of TTF-CA (panel a) and DMeTTF-CA (panel b) as a function of temperature in the spectral region and polarization where the C=O antisymmetric stretching occurs. The upper x-axis scale is given directly in terms of ionicity to ease the comparison. It is clearly seen that the temperature evolution of ρ is different in the two cases. In TTF-CA, the ionicity gradually increases from about 0.2 at room temperature to about 0.3 at 81 K. Below 81 K, ρ jumps to about 0.5, and gradually increases up to 0.6 at 15 K ([10], not shown in the Figure). Also in DMeTTF-CA ρ increases gradually by lowering T , reaching ~ 0.3 at 64 K. Then there is a small jump and in a restricted temperature interval the C=O stretching band splits (arrows in Figure 1), indicating the presence of two differently charged species. Below 55 K there is again a single ionicity of about 0.4, which increases again by lowering T , but without crossing the 0.5 N-I borderline [17].

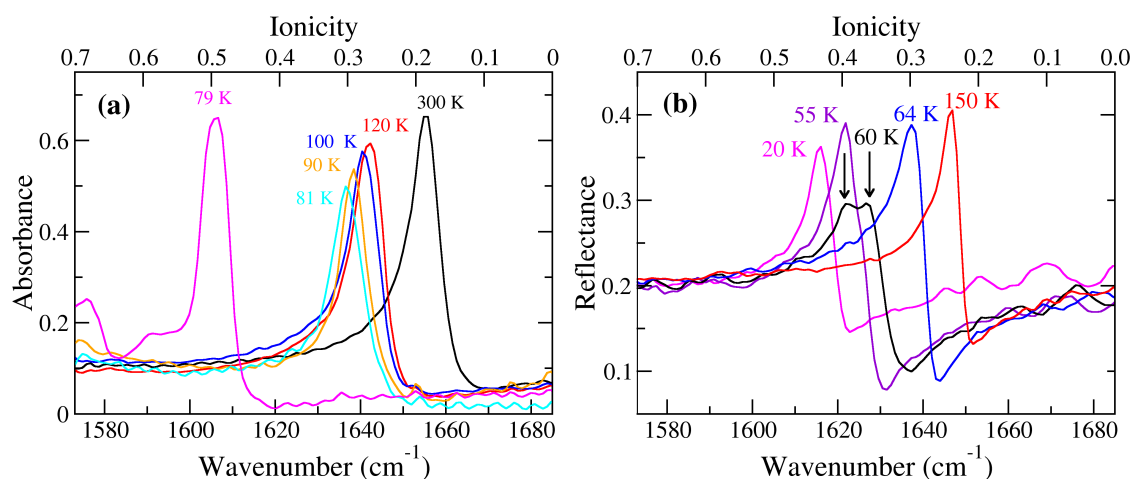


Figure 1. Temperature evolution of the IR spectra polarized perpendicular to the stack axis in the C=O antisymmetric stretching spectral region. (a) TTF-CA; (b) DMeTTF-CA, adapted from [17].

The IR spectra polarized parallel to the stack also offer a very convenient and sensitive probe of stack dimerization [21,22]. In the absence of dimerization (“regular” stack), each molecule resides on an inversion center, and the so-called mutual exclusion rule holds: Raman active intra-molecular vibrations are inactive in IR and vice-versa. When the stack dimerizes, and the inversion center is lost, the totally-symmetric vibrations become also visible in IR. However, due to the above mentioned e-mv interaction, they mix with the nearby CT electronic transition, borrowing huge intensity along the stack (vibronic, or e-mv induced bands).

Figure 2 nicely illustrates the above mechanism for detection of stack dimerization for the two CT crystals at hand. Panel (a) shows that the absorption spectra of TTF-CA polarized along the stack exhibit little change in passing from 86 to 80 K. However, the spectrum at 79 K, just below the critical temperature, shows the sudden appearance of very strong bands around 1550, 1330 and 950 cm^{-1} (actually the spectrum is saturated at these frequencies), in correspondence with TTF and CA totally symmetric modes with the strongest e-mv coupling constants [10]. Analogous strong bands arise in the low-temperature spectra of DMeTTF-CA (panel (b)), but in this case the insurgence of the bands is more gradual, starting around 60 K, and progressively gaining intensity.

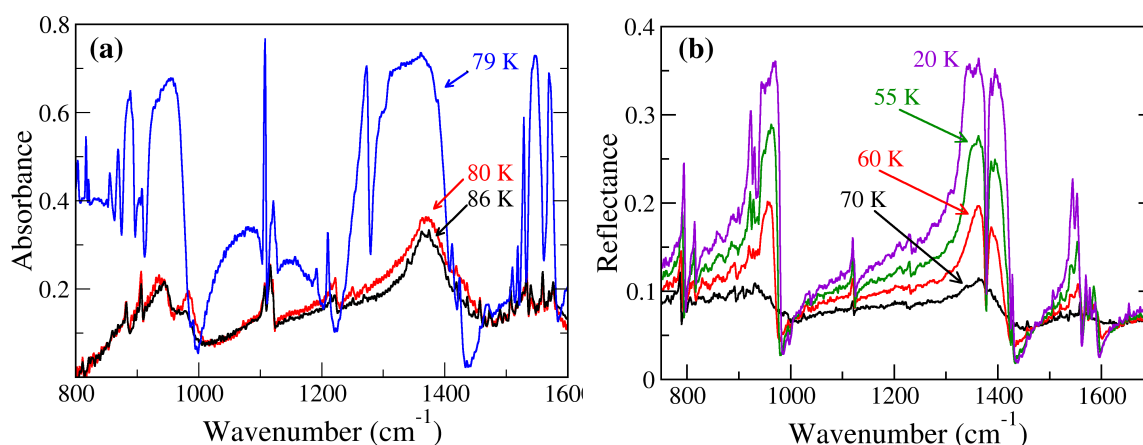


Figure 2. IR spectra polarized along the stack axis as a function of temperature. (a) TTF-CA (this work); (b) DMeTTF-CA, from [17].

Direct structural information comes of course from X-ray analysis. In the case of TTF-CA, neutron diffraction experiment showed that the crystal structure evolves from $P2_1/n$ (C_{2h}^5), with two DA pairs (two stacks) in the unit cell, to P/n (C_s), always with $Z = 2$. The symmetry breaking at $T_c = 81$ K involves the loss of the inversion center (stack dimerization) and of the screw axis. The order parameter for the dimerization has B_u symmetry in the C_{2h}^5 phase, and the electric dipoles from A to D have the same orientation in the two stacks, so the structure is ferroelectric [25]. The NIT of DMTTF-CA appears to be more complex. The room temperature structure is $P\bar{1}$, with just one DA pair, and each molecule resides on the inversion center (regular stack) [26]. The phase transition yields a cell doubling, with two dimerized stacks per unit cell. At present, there is no agreement between the two structural determinations of the low temperature phase, as one indicates that the two stacks are equivalent, with anti-ferroelectric arrangement ($P\bar{1}$) [14], and the other that the two stacks are inequivalent ($P1$ symmetry), with ferrielectric arrangement [26]. We remark that the structural determinations must be performed with great accuracy to establish the precise nature of the structure, and in particular the stack dimerization, which is very small: If we define the dimerization amplitude δ as the ratio between the difference and the sum of the DA, AD distance along the stack, we get $\delta = 0.03$ for both TTF-CA and DMeTTF-CA. As shown by Figure 2, such small δ yields huge spectroscopic effects.

Once the crystal structure of the low-temperature phase has been determined, the temperature evolution of the dimerization amplitude can be followed by looking at the intensity of selected X-ray

reflection spots. Figure 3 compares the temperature evolution of the TTF-CA and DMeTTF-CA Neutral-Ionic phase transition. The (a) and (d) panels report the ρ order parameter, as estimated from the frequency of the C=O antisymmetric stretching, the other panels report the T evolution of the δ order parameter, estimated by the intensity of the IR e-mv induced bands and from the intensity of the selected X-ray spots.

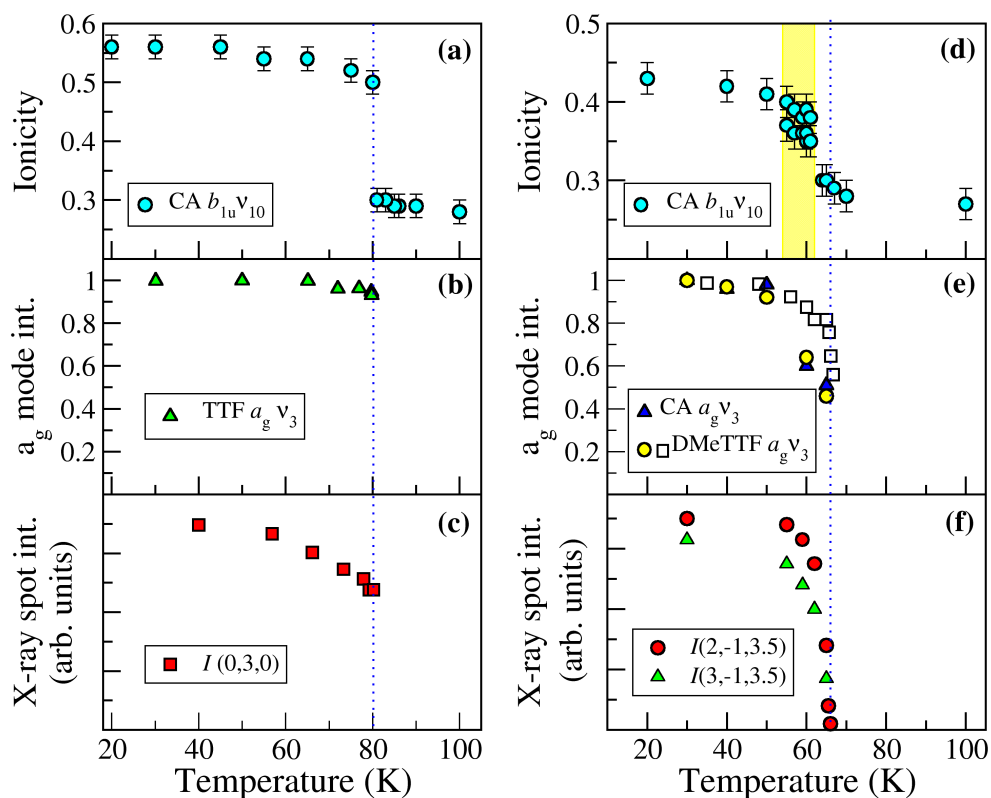


Figure 3. Temperature evolution of the Neutral-Ionic transition of TTF-CA (left panels) and DMeTTF-CA (right panels). Panels (a) and (d) : Ionicity, as measured by the frequency of the C=O antisymmetric stretching; Panels (b) and (e), Normalized dimerization amplitude, as estimated from the IR intensity of the e-mv induced modes; Panels (c) and (f): Dimerization amplitude as estimated by the intensity of X-ray spots. Panels (b) and (c) are from [16], panels (d)–(f) are from [17].

Figure 3 highlights the differences between TTF-CA and DMeTTF-CA. In TTF-CA, the transition is first order, with simultaneous jump in the ionicity and setting of a finite dimerization amplitude at T_c (indicated by dotted lines in the Figure). In DMeTTF-CA the phase transition implies only a limited change of ρ , that remains well below the 0.5 N-I borderline, on the *neutral* side. So it would be better to consider the transition as valence instability, rather than a “true” NIT. More importantly, cell doubling and stack dimerization appear to constitute the driving force of the transition, since the major charge rearrangement follows, by a few degrees K, the onset of cell doubling and stack dimerization. We can envision a scenario in which the dimerization and cell doubling lead to a better molecular packing, with an increase in the Madelung energy and consequent small, almost continuous change in ρ . The presence of slightly differently charged molecular species before the dimerization/cell doubling has reached completion (yellow shaded area in panel (d)) fits quite naturally into this picture.

2.1.2. Soft Phonon(s)

Whereas the role of intermolecular (lattice) phonons in setting up the phase transition of DMeTTF-CA is obvious, it is not so in the case of the first-order, discontinuous transition of TTF-CA.

Indeed, the details of the microscopic mechanism of TTF-CA have been a matter of debate since long, as hydrogen bonding [27] or lattice-relaxed CT exciton strings (LR-CT) [28] were suggested to add to the role of Madelung energy in establishing the transition. On the other hand, dimerization also implies the presence of intermolecular Peierls phonon(s), coupled to electrons through the modulation of the hopping integrals t_{DA} (e-ph coupling [21,22]). In the case of mixed stack Peierls soft phonons occur at the zone center and should be detectable in the far-IR. Early attempt to detect the Peierls mode and its softening by powder IR spectra failed to provide definite experimental evidence [29]. Curiously, a more convincing identification of a soft mode in the pre-transition regime of TTF-CA came from a careful parallel IR and Raman analysis in the spectral region of intra-molecular vibrations [30].

In the previous Subsection we have seen that below T_c the IR spectra polarized parallel to the stack axis are characterized by very strong bands corresponding to totally symmetric modes of the D and A molecules. These Raman active modes are coupled to delocalized electrons through the modulation of on-site energy (e-mv or Holstein coupling [21]), and become active also in IR, with huge intensity, when the stack dimerizes, losing the inversion center (Figure 2). On the other hand, IR bands in close proximity of these totally symmetric vibrations are also visible *above* T_c , when the stack is regular and the totally symmetric vibrations are visible only in Raman. As shown in Figure 4, these IR bands, labeled 'A' and 'B', occur in pairs, at frequencies symmetrically above and below that of the associated Raman band - hence the name of "sidebands" [30]. Their frequency difference with respect to the Raman band is the same for different totally symmetric modes, and decreases with T . Therefore the A and B sidebands are quite naturally interpreted as difference and sum combination bands, respectively, between molecular totally symmetric vibrations and the Peierls phonon. Indeed, both types of phonons are coupled to CT electrons, hence are coupled together.

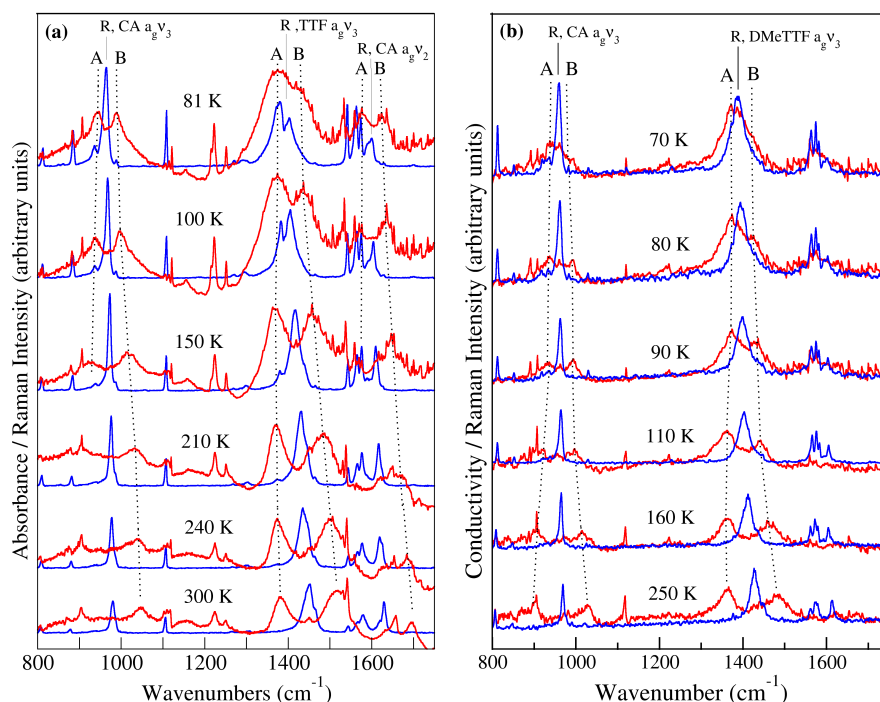


Figure 4. Comparison of Raman (blue line) and IR spectra polarized parallel to the stack (red line) for (a) TTF-CA [30] and (b) DMeTTF-CA [17]. The dotted line is a visual aid to follow the temperature evolution of A and B IR "sidebands" discussed in the text. The corresponding Raman bands are labeled by R and the assignment is reported on top.

The frequency of the soft mode can then be derived by taking the difference between the frequency of the B band ($\Delta\omega_+$) or of the A band ($\Delta\omega_-$) with respect to the corresponding Raman

band. Alternatively, one can take half the difference between the B and A bands, since they have equal distance, within the experimental error, from the Raman band. Figure 5 reports the temperature evolution of the frequency of the soft mode of TTF-CA ([30]) and of DMeTTF-CA ([17]) derived in this way. The temperature evolution of the frequency follows the behavior expected for a soft mode, $\Delta\omega = \omega_0\sqrt{T - T_{\text{Peierls}}}$ (dashed lines in Figure 5). It is then evident that a Peierls soft mode is present in both compounds. However, in TTF-CA the first order transition takes place well before the soft mode goes to zero, whereas in DMeTTF-CA the transition occurs upon almost complete softening. Of course, also the final state is different, because in TTF-CA one ends on the Ionic side, with a ferroelectric arrangements of the two “dimers” in the unit cell [25], whereas in DMeTTF-CA there is cell doubling, and the resulting two “dimers” are arranged in a ferrielectric or antiferroelectric manner [17,26].

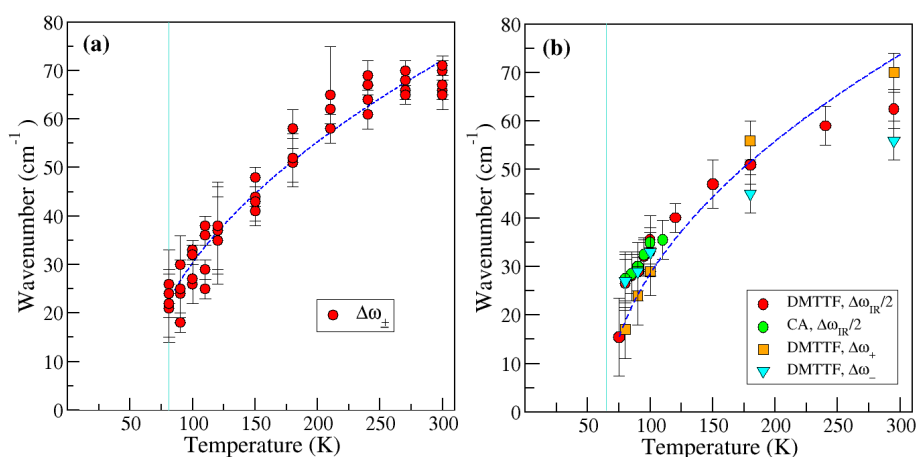


Figure 5. Temperature evolution of the frequency of the effective soft mode as derived from the frequency of the A and B sidebands (see text and Figure 4). The dashed blue line is the best fit of the experimental points with the curve $\Delta\omega = \omega_0\sqrt{T - T_{\text{Peierls}}}$. Panel (a): TTF-CA, from [30]; Panel (b): DMeTTF-CA, from [17].

Direct spectral observation of the Peierls mode throughout the phase transition can be obtained by single crystal far-IR spectra polarized along the stack, but these are difficult to obtain. Absorbance spectra require relatively large but very thin crystals, whereas reflectance spectra require a careful extrapolation to zero-frequency to perform the Kramers-Kronig transformation to the more easily interpreted conductivity spectra. Low-frequency Raman spectra are easier to measure and interpret, but the Peierls mode is Raman active only in the low-temperature, dimerized stack phase. As a matter of fact a complete IR and Raman study has been performed only for the TTF-CA [31,32], whereas only Raman spectra are available for DMeTTF-CA [17]. Here we shall limit ourselves to report in some detail the analysis for TTF-CA, including some unpublished Raman spectra, deferring the reader to the original paper for DMeTTF-CA [17].

According to neutron diffraction [25], room temperature quasi-neutral TTF-CA crystallizes in the $P2_1/n$ (C_{2h}^5) space group. Below T_c , in the quasi-ionic phase, the C_2 axis and the inversion center are lost, the space group being Pn (C_s^2). The stack axis is the a axis, and the unit cell contains two formula units. Symmetry arguments [31] show that in the N phase the (mostly intermolecular, or lattice) phonons able to modulate the hopping integral t_{DA} belong to the B_u symmetry, and are IR active with oscillating dipole moment along a . Correlation between the C_{2h} and C_s factor group shows that on crossing the N-I borderline the B_u phonons become A' , active both in IR and Raman. We then start from the more accessible Raman spectra of the low-temperature phase.

The assignment of the A' low-frequency modes is reported in detail in [31]. Figure 6 reports the temperature evolution of the Raman spectra and frequencies. The Figure shows that upon approaching the critical temperature from below, there is a clear softening of the phonon observed at about 90 cm^{-1}

at 15 K, that moves to about 80 cm^{-1} just before the transition (marked by an arrow in the Figure). So the identification of the Peierls mode is easy in the ionic phase. Notice however that another phonon, at about 75 cm^{-1} at 15 K, starts to show some frequency lowering above 65 K, when the 90 cm^{-1} Peierls mode become closer due to the softening. Indeed, when the two phonons approach in frequency, they mix together, and the higher frequency phonon transfers part of its e-ph coupling strength to the lower frequency one. The phenomenon is limited in the ionic phase since the frequency span of the Peierls phonon, a little more than 10 cm^{-1} , is small in the relevant temperature interval of about 70 K. We may expect, and indeed find, that the mode mixing and transfer of the coupling strength progressively to lower frequency phonons will be much more pronounced in the high temperature neutral phase, since the frequency span of the soft mode found by the analysis of the sidebands is about 50 cm^{-1} from 300 K to 81 K (Figure 5a).

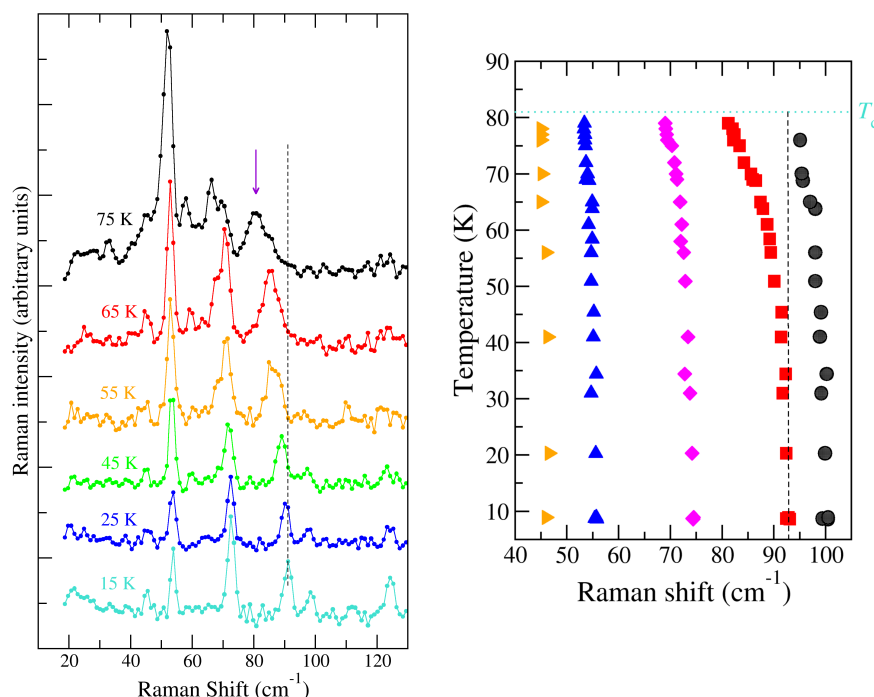


Figure 6. Temperature dependence of the low-frequency Raman spectra of the low-temperature, quasi-ionic phase of TTF-CA, showing the softening of the mode around $90\text{--}80\text{ cm}^{-1}$ (marked by an arrow) as $T_c = 82\text{ K}$ is approached from below. The temperature evolution of the peak frequencies of the main Raman bands is reported on the right panel.

Figure 7 shows the temperature evolution of the low-frequency IR conductivity spectra polarized along the stack axis of TTF-CA in the neutral phase. The spectra have been obtained by Kramers-Kronig transformation of the reflectivity collected between 6000 and 5 cm^{-1} . The high-frequency extrapolation has taken advantage of the literature data up to $14,000\text{ cm}^{-1}$, whereas the data below 5 cm^{-1} were extrapolated to fit the known value of the static dielectric constant [32]. A first look at the conductivity data does not allow to identify the presence of a soft mode. Rather, one notices a red shift of the overall spectral weight as temperature is lowered. A spectral fit with a series of six Lorentzian peaks yields to the temperature evolution of the peak frequency reported in the right side of Figure 7. Here one can observe the softening of the lowest frequency mode, which is barely visible in the spectra due to its large bandwidth. In addition, the overall softening and frequency does not agree with that derived from the analysis of the sidebands detected in the high frequency region of the spectrum (Figure 5a). A theoretical analysis is needed to properly interpret the temperature evolution of the low-frequency

IR conductivity spectra. The details of such analysis is reported in [32], and here we limit ourselves to a short summary.

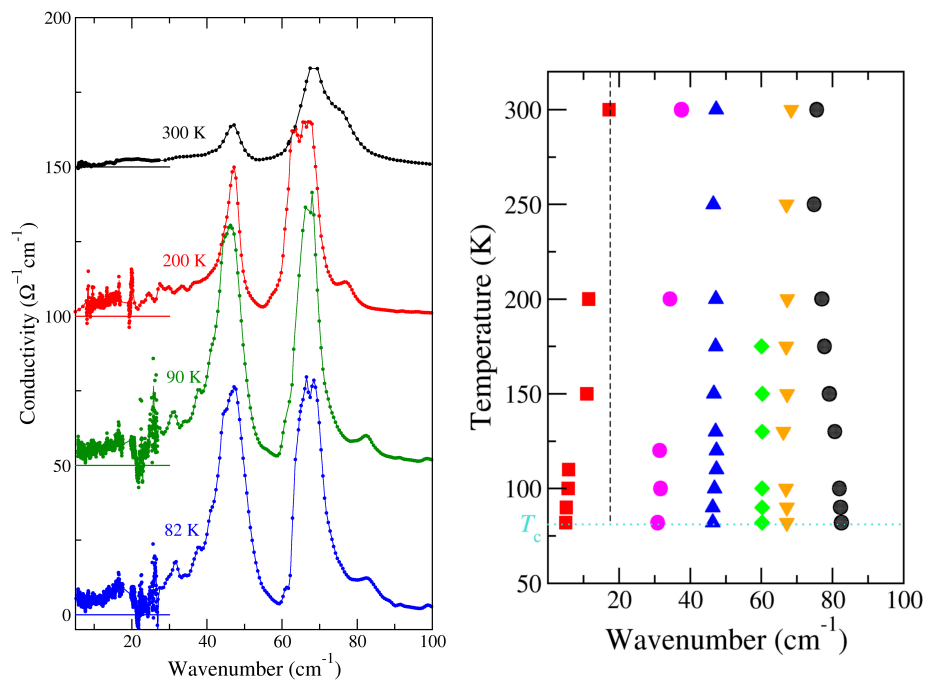


Figure 7. Temperature evolution of the low-frequency conductivity spectrum polarized along the stack axis and of the relevant IR frequencies in TTF-CA neutral phase. Adapted from Ref. [32].

In the first step the frequencies and normal coordinates of TTF-CA low-frequency phonons at 300 K and at 40 K are calculated by the so-called Quasi Harmonic Lattice Dynamics (QHLD) method, by adopting an empirical intermolecular atom-atom potential, as fully described in [31]. Such potential does not include the CT interaction, so that the frequencies and eigenvectors are zero-order reference frequencies in the absence of Peierls coupling. In other words, they correspond to an hypothetical state where the electronic excitations are moved to infinite energy. The e-ph (Peierls) coupling constants are then calculated by:

$$g_i = \sqrt{\frac{\hbar}{2\omega_i}} \left(\frac{\partial t_{DA}}{\partial Q_i} \right)_{eq} \quad (1)$$

where t_{DA} is the CT integral between adjacent DA molecules along the stack, and Q_i is the reference normal coordinate for the i -th phonon with frequency ω_i and wavevector $\mathbf{q} = 0$. The CT integral and its variation with Q_i is calculated by the extended Hückel method [31]. As an example of the involved phonons, Figure 8 shows the eigenvectors of two strongly coupled reference phonons of neutral (B_u , right panel) and ionic (A' , left panel) TTF-CA, calculated at 99.4 and 107.1 cm^{-1} , respectively. The B_u phonon, as expected [25], implies an in-phase (ferroelectric) D-A oscillation along the two stacks in the unit cell. The A' phonon, on the other hand, also involves a rotational motion of the two molecules.

Calculations show that other modes, besides those pictorially reported in Figure 8, are appreciably coupled to CT degrees of freedom, leading to a typical *multi-mode* coupling problem, where the different vibrations are mixed together, according to the following force constant matrix:

$$F_{ij}(T) = \omega_i \omega_j \delta_{ij} - \sqrt{\omega_i \omega_j} g_i g_j \chi_b. \quad (2)$$

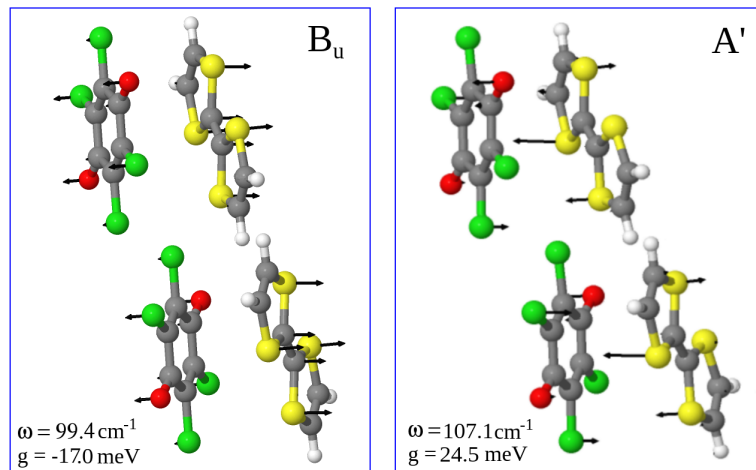


Figure 8. Eigenvectors, reference frequencies and e-ph coupling constants of two strongly coupled lattice mode of TTF-CA, one for the neutral phase (B_u) and the other for the ionic phase (A').

Here, ω_i and g_i are the reference frequencies and coupling constants, and χ_b is the electronic response to the phonon perturbation. As usual, the eigenvalues of the force constant matrix yield the squared vibrational frequencies of the coupled problem, Ω_j^2 , while the eigenvectors are the relevant normal coordinates Q_j . The structure of the force constant matrix in Equation (2) clearly points to a softening of coupled modes, with effects that increase with the electronic susceptibility. Similarly, the absolute values of the off-diagonal elements of the force constant matrix, responsible for the e-ph induced mixing of vibrational modes, also increase with χ_b : The description of the normal modes varies with the strength of e-ph coupling in a multi-mode system.

Equation (2) has been applied to the neutral phase of TTF-CA by properly calibrating the electronic susceptibility, χ_b , previously calculated in [33] by exact solution of a modified Hubbard model with parameters optimized to mimic the behavior of TTF-CA. The diagonalization of the force constants matrix in Equation (2) quite naturally explains why—although several phonons are coupled to the CT electrons—the observed red shifts of vibrational bands upon approaching NIT is fairly small. The mixing of coupled vibrations, driven by the off-diagonal matrix elements in the force constant matrix, increases with lowering T , due to the increase of the electronic susceptibility χ_b . The normal coordinates of the coupled system Q_j then acquire a T -dependence:

$$Q_j(T) = \sum_i l_{ij}(T) Q_i, \quad (3)$$

where Q_i are the T -independent reference normal coordinate, and $l_{ij}(T)$ are the eigenvectors obtained by diagonalizing the force constant matrix in Equation (2) with the calibrated T -dependent χ_b . A T -dependent effective coupling constant can then be assigned to each normal mode of the coupled system:

$$G_j(T) = \sum_i l_{ij}(T) g_i \sqrt{\frac{\omega_i}{\hbar}}, \quad (4)$$

As a result of the χ_b increase upon approaching NIT, the coupling strength, as measured by $[G_j(T)]^2$, progressively transfers from higher to lower frequency modes, finally yielding substantial softening of the lowest frequency phonon.

The Peierls coupling not only affects vibrational frequencies, but also oscillator strength and bandwidths, as shown by the following equations derived in [32]:

$$f_j(T) = \frac{m_e d^2}{t_{DA}^2} [G_j(T)]^2 \left(\frac{\partial P}{\partial \delta} \right)^2, \quad (5)$$

$$\Gamma_j(T) = k \frac{[G_j(T)]^2}{\Omega_j} + \Gamma_j^0 = k \eta_j(T) + \Gamma_j^0. \quad (6)$$

In Equation (5) m_e is the electronic mass, d the equilibrium distance between D and A molecules, P the electronic polarizability and δ the dimerization amplitude, whereas in Equation (6) k is an adjustable parameter and Γ_j^0 is the intrinsic vibrational linewidth. Thus the progressive transfer of the coupling strength, $[G_j(T)]^2$, from higher to lower frequency modes on lowering T , justifies the progressive transfer of the softening, the concomitant transfer of oscillator strength, and a broadening of the IR bands related to the anharmonicity induced by the e-ph coupling.

The above described effects of Peierls coupling fully explain the complex temperature evolution of TTF-CA spectra in the neutral phase (Figure 7), as illustrated in Figure 9. In this Figure the dotted lines show the temperature dependence of the frequencies of the six Peierls coupled modes below 100 cm^{-1} , as obtained from the fitting procedure. Superimposed to the frequency curves we report, for selected temperatures, the calculated single Lorentzians associated with each phonon. From Figure 9 one can appreciate the interplay between the frequency softening, the spectral weight redistribution, and the bandwidth increase. In fact, all the phonons are coupled together through their common interaction with the electronic system (Equation (2)), and with lowering temperature ρ increases leading to a larger electronic delocalization and hence to an amplified χ_b . As a consequence, phonons soften as approaching NIT, but when two phonon frequencies get close they get mixed together and the softening is “transferred” to the lower frequency phonon. The description of the normal modes evolves with temperature and the coupling strength is progressively transferred to the lower frequency modes as the phase transition is approached. Indeed all the coupling strength would be eventually transferred to the lowest frequency phonon, if the first order $N-I$ instability would not take over before the frequency of this phonon becomes zero.

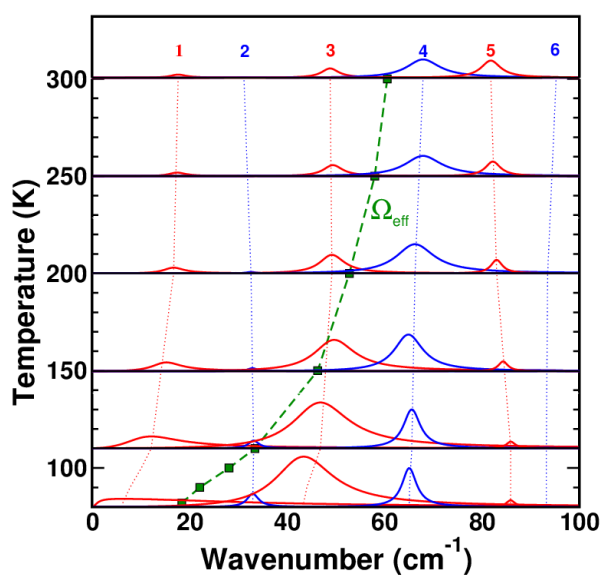


Figure 9. Temperature dependence of the frequency of the six lowest frequency Peierls coupled phonons, after the fitting to reflectivity spectra. For 300, 250, 200, 150, 110, and 82 K the calculated individual Lorentzian bandshapes are also shown. The green squares connected by a dotted line indicate the frequency of the effective Peierls mode, calculated by Equation (7) (From [32]).

At the light of the above multimode analysis of Peierls modes, the soft phonon inferred from the analysis of the mid-IR “sidebands” (Figure 5) must correspond to an *effective* Peierls phonon, resulting

from the weighted contribution of the several Peierls coupled mode, as derived from the following expression:

$$\Omega_{\text{eff}} = \frac{\sum_j \eta_j \Omega_j}{\sum_j \eta_j}, \quad (7)$$

where each frequency is weighted by η_j , the same factor entering the definition of vibrational linewidth in Equation (6).

In Figure 9 the frequency obtained from Equation 7 (green squares connected by a dashed line), is superimposed to the frequencies of the six phonons below 100 cm^{-1} . It is seen that Ω_{eff} follows the softening and the shift of spectral weight described by the Figure. The comparison of the computed Ω_{eff} with the frequency obtained from the analysis of combination bands in the mid-IR region is shown on the right side of Figure 10. The agreement between these two totally independent set of data is impressive, and strongly supports the interpretation of the spectroscopic data in terms of a soft mode. In the left side of the Figure we report, for completeness, the softening of the A' phonon around $80\text{--}90 \text{ cm}^{-1}$ of TTF-CA ionic phase. Calculations analogous to those just described for the neutral phase show that several phonons are coupled to the electronic system also on the ionic side [34], but that for the limited T and ρ interval the transfer of the coupling strength to lower frequency phonons is not appreciable. Therefore in this case the single A' phonon coincides with the effective Peierls phonon.

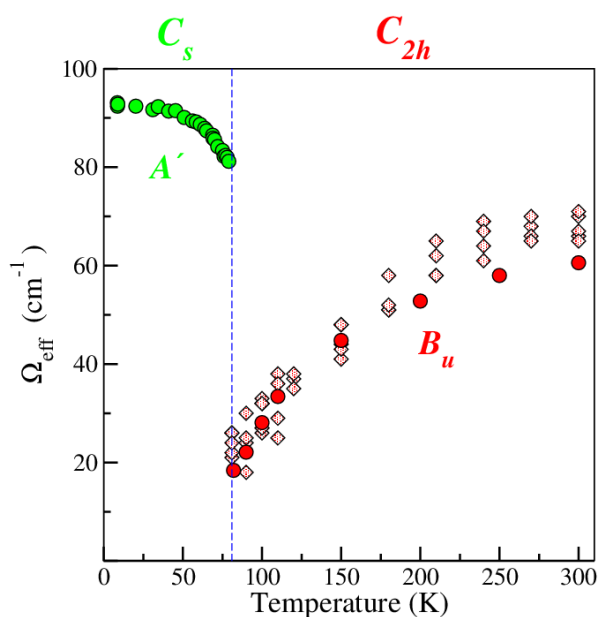


Figure 10. Effective soft phonon frequency of TTF-CA, above (red circles) and below (green circles) the NIT. The shaded red diamonds are the $\Delta\omega$ of the mid-IR sidebands of Figure 5a.

To summarize, definite evidence has been found for the presence of soft phonon(s) inducing the dimerization of the stack through the Peierls mechanism. The presence has been ascertained not only in the case DMETTF-CA, where Peierls coupling is likely the driving force of the transition, but also in the case of TTF-CA, where NIT appears to be first-order, Mott-like and driven by the Madelung energy. The Peierls phonon(s), through their coupling with the CT electron, cause a low-frequency charge oscillation along the stack. As the ionicity increases and the CT electron becomes more delocalized, the importance of the charge oscillation increases, and at the same time the Peierls phonon becomes more and more anharmonic. As we shall see in the next Subsection, this low-frequency anharmonic charge oscillation has important consequences on the phenomenology of NIT in the proximity of the transition.

2.1.3. Anomalies in the Proximity of NIT

NIT is an electronic phase transition, implying a collective charge transfer from D to A, associated with a structural or Peierls transition driven by e-ph interaction. It is no surprise that a set of peculiar phenomena or anomalies has been observed in its proximity, like for instance the large increase of the dielectric constant [16,18] or the nonlinear electric transport [35]. A number of theoretical concepts have been proposed with the aim of explaining the observed anomalies: Apart from domain walls or topological solitons separating regions with opposite dimerization [36,37], Nagaosa developed the concept of neutral-ionic domain walls (NIDW) separating domains of LR-CT [38]. However, most observed anomalies can be accounted by a simple model considering the coupling of a soft mode to a correlated electronic system. The details of the model and of the theoretical interpretation are left to another feature paper in the present special issue of *Crystals* [39]. Here we shortly summarize the relevant phenomenology in the case of TTF-CA and DMeTTF-CA.

Besides vibrational and structural analysis, the measurement of the dielectric constant ϵ_1 is an additional important tool to investigate NIT, as $\epsilon_1(T)$ shows a divergent-like peak, or cusp anomaly, characteristic of ferroelectric or antiferroelectric transitions. The dielectric constant anomaly of TTF-CA [16] and DMeTTF-CA [18] is shown in Figure 11. Notice the different full-scale value in the two cases, the cusp anomaly of TTF-CA being about twice of the DMeTTF-CA one. The peak divergence occurs precisely at T_c in both cases. The dielectric anomaly was initially explained as due to the quantum motion of NIDW [16]. Modern polarization theory offers an alternative explanation [33], although the low-frequency charge-oscillations induced by the soft mode have been shown to give by far the largest contribution [33,39].

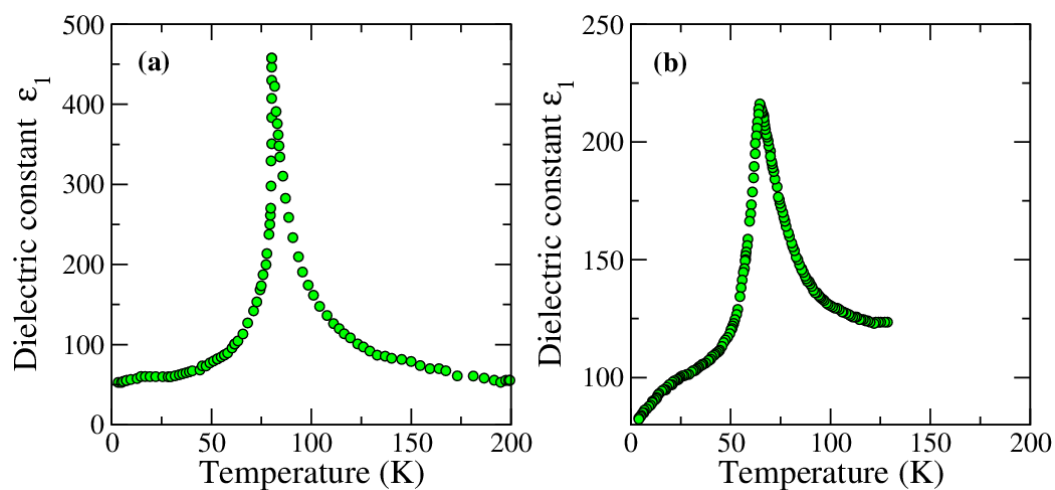


Figure 11. Temperature dependence of the real part of the dielectric constant (measured at 30 kHz) of: (a) TTF-CA, adapted from [16]; (b) DMeTTF-CA, adapted from [18].

Evidence of the elusive LR-CT in the proximity of NIT has been sought by a very careful analysis of the diffuse X-ray scattering as a function of temperature [40,41]. The sharp Lorentzian-shaped diffuse X-ray signal collected along one spatial direction (Figure 12) implies the lack of long-range correlation order. The explanation in terms of a strong dispersion of zone-center optical phonons like those depicted in Figure 8 was considered unlikely. However, e-ph coupling is very effective in 1D, in this case giving rise to a drastic softening precisely at the zone-center (Figure 5). Thus the diffuse X-ray of TTF-CA and DMeTTF-CA can be interpreted [39,42] analogously to the well-known Kohn anomaly of 1D metals [43].

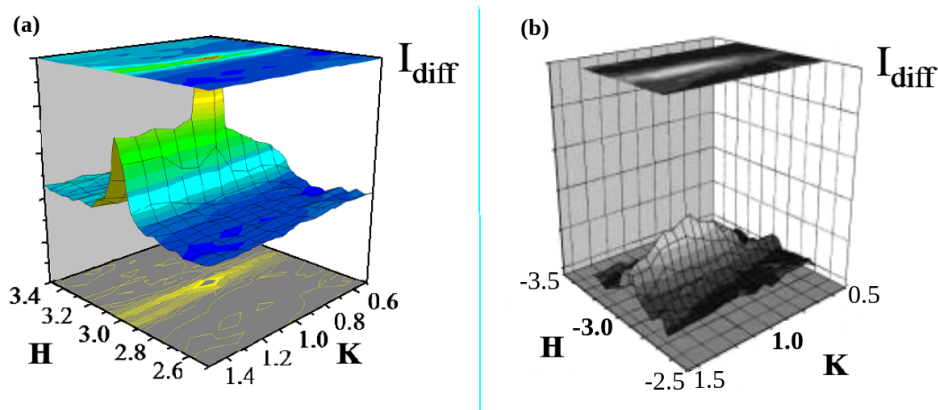


Figure 12. Diffuse scattering intensity. (a) TTF-CA, $T = 84$ K, scattering around $(3\ 1\ -1)$ in the (a^*b^*) plane. Reproduced with permission from [40]. (b) DMeTTF-CA, $T = 100$ K, scattering around $(-3\ 1\ 0.5)$ in the (a^*b^*) plane. Reproduced and adapted with permission from [41].

The search for the so-called Goldstone mode [44] was among the motivations of the detailed study of intensity changes close to the exciting line of the Raman spectrum of TTF-CA and DMeTTF-CA. The Goldstone mode is a collective very low-frequency mode associated with the spontaneous breaking of a (continuous) symmetry, in the case of crystals the breaking of the translational order. Panel (b) of Figure 13 shows that in the DMeTTF-CA Raman spectrum around the NIT there is a clear background increase starting from about 90 cm^{-1} towards zero-frequency. An analogous effect is observed in TTF-CA (panel (a) of the Figure), although less pronounced due to the sharp discontinuous nature of the transition in that case. A detailed theoretical analysis [39,45] has shown that the broad low-frequency Raman signal can be interpreted as the overtone of the overdamped soft dimerization mode, and not as the Goldstone mode. The Raman feature actually signals the fluctuations of the electronic polarizability, which diverges at the NIT (dielectric catastrophe).

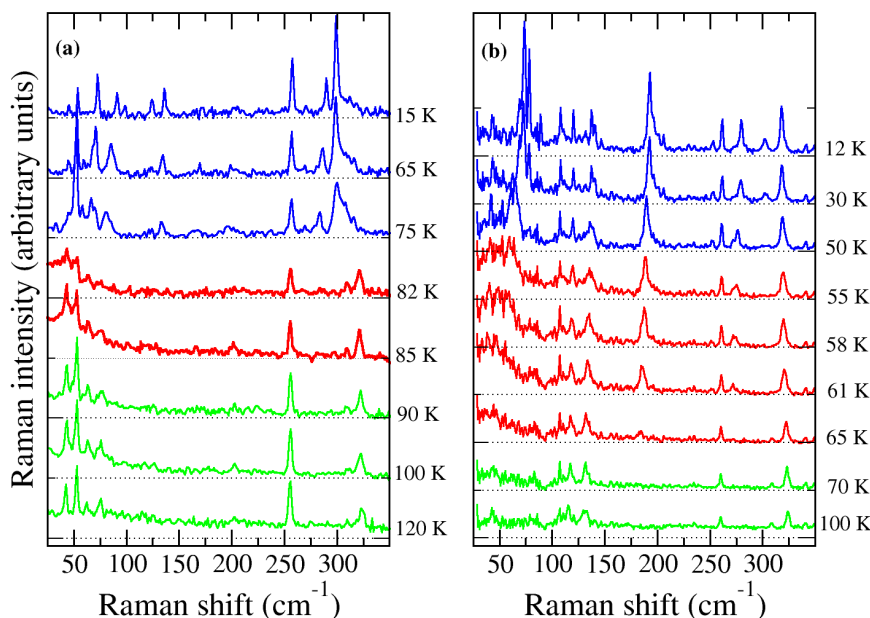


Figure 13. Temperature evolution of the low-frequency Raman spectra of TTF-CA (panel (a)) and DMTTF-CA (panel (b)), measured with incident and scattered light polarized along the stack axis. The spectra drawn in red are those collected in the proximity of the phase transition, where the low-frequency background increase is evident.

2.2. TMB–TCNQ

The temperature induced NIT of 3,3',5,5'-tetramethylbenzidine–tetracyanoquinodimethane (TMB–TCNQ) was reported several years ago [46]. The phase transition occurs around 200 K, with large hysteresis and with a ρ variation of about 0.1 just around the N-I borderline [46]. Despite the many similarities with TTF–CA, and the convenient high temperature of the transition, no further investigation has been performed, except for a study on the thermal hysteresis, where it was shown that the crystals break at the transition [47]. A recent reinvestigation [19], that we summarize here, has helped to clarify some issues and to better characterize the phase transition and its mechanism.

Figure 14 compares the polarized IR absorption spectra above and below the phase transition in the spectral regions of interest. The spectra polarized perpendicular to the stack (left panel) shows that the charge sensitive bands shift very little at the transition. Iwasa et al. used the TCNQ $b_{1u}\nu_{19}$ CN stretching frequency to estimate ρ , obtaining a change from 0.59 to 0.69 at the transition [46]. However, it is well known that the CN stretching frequency gives unreliable (generally overestimated) values of ρ since it suffers from uncertainty about the correct assignment, and is subject to extrinsic effects due to the interactions with the surrounding molecules [48]. For this reason, Castagnetti et al. used the well tested charge sensitive TCNQ $b_{1u}\nu_{20}$ C=C stretching, that in TMB–TCNQ moves from 1532 to 1528 cm^{-1} , corresponding to a ρ increase from 0.29 to 0.41 [19]. Therefore TMB–TCNQ remains on the neutral side also in the low-temperature phase.

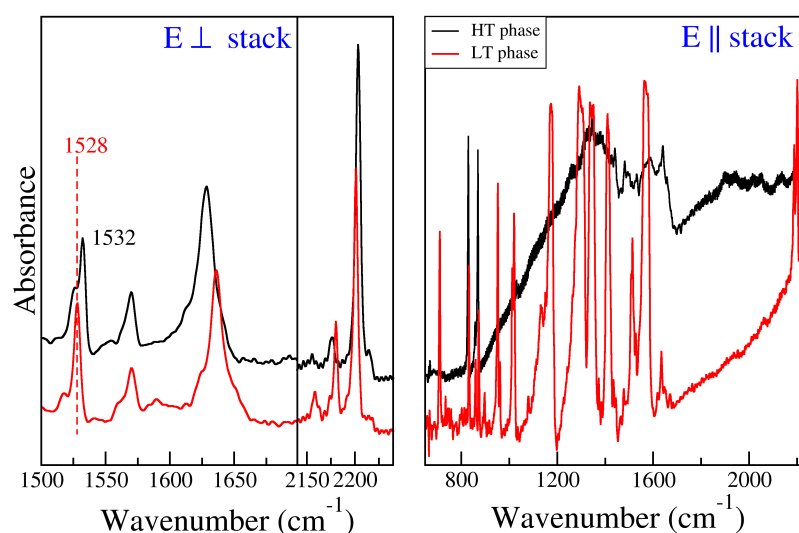


Figure 14. IR absorption spectra of TMB–TCNQ polarized perpendicularly and parallel to the stack axis, above (HT) and (LT) below the phase transition. From [19].

Figure 14 shows that the low-temperature TMB–TCNQ IR spectrum polarized along the stack axis (red trace in right panel of Figure 14) is dominated by a set of new, very strong bands, clearly due to e–mv coupling. These bands unambiguously indicate the dimerization of the stack at the phase transition. The spectrum above the phase transition (black trace in the Figure) shows a very broad band, with a strange shape. The increase of the baseline is due to the proximity of the onset of the very intense CT electronic transition, also polarized along the stack axis, and the very strange and complex band-shape can be explained by considering that, as in TTF–CA [30], we are in the presence of combination modes between the Raman active totally symmetric intra-molecular modes and the low-frequency inter-molecular Peierls mode(s). In TTF–CA, these modes could be identified, since the totally symmetric modes coupled to the CT electron are relatively few and isolated. In the present case between 1000 and 1600 cm^{-1} we have instead many strongly coupled totally symmetric modes,

as seen in the low-temperature spectra, so that the combinations modes overlap and coalesce, giving rise to the strange band-shape.

The Raman active totally symmetric modes are coupled to delocalized electrons [21,22], and in mixed stack crystals the linear dependence of their frequency from ρ is lost. Nevertheless, a rough estimate of ρ can be obtained by taking into account the perturbing effect of e-mv interaction through an appropriate model. The (a) panel of Figure 15 shows that in TMB-TCNQ the TCNQ $a_g\nu_4$ mode shifts from 1418 to 1411 cm^{-1} at the phase transition. For a regular chain like room-temperature TMB-TCNQ we can use the trimer model to estimate ρ , and by disregarding the interaction among e-mv coupled modes (isolated band approximation), the perturbed frequency Ω is given by [49]:

$$\Omega_{e-mv}^t = \sqrt{(\omega_N - \Delta\varrho) \left[(\omega_N - \Delta\varrho) - \frac{4g^2}{\omega_{CT}} \varrho(1 - \varrho)^2 \right]} \quad (8)$$

where ω_N is the vibrational frequency of the neutral molecule, Δ the ionization frequency shift, g the e-mv coupling constant and ω_{CT} is the frequency of the CT transition. Below the transition, when the stack is dimerized, the dimer model can be adopted [49]:

$$\Omega_{e-mv}^d = \sqrt{(\omega_N - \Delta\varrho) \left[(\omega_N - \Delta\varrho) - \frac{4g^2}{\omega_{CT}} \varrho(1 - \varrho) \right]} \quad (9)$$

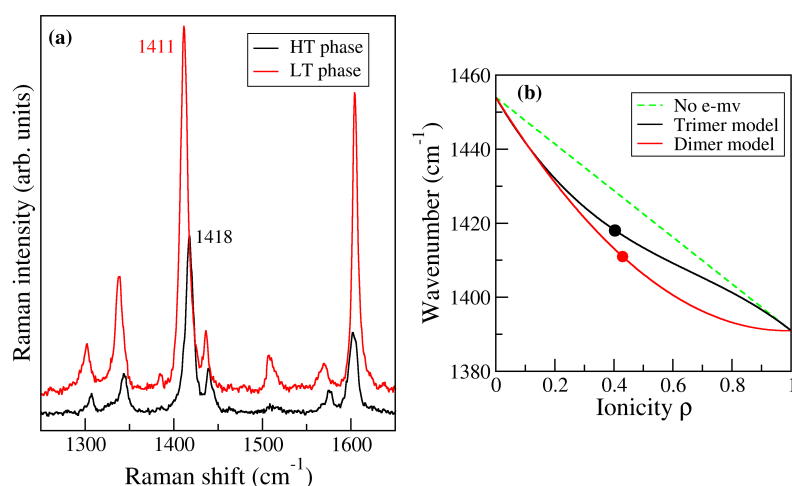


Figure 15. (a): Raman spectra of TMB-TCNQ above (HT) and below (LT) the phase transition, from [19]; (b): plot of Equations (8) and (9) for the TCNQ $a_g\nu_4$ mode with the parameters given in the text. The dashed green line shows the linear dependence in the absence of e-mv coupling.

The above two equations are plotted for the $a_g\nu_4$ mode in panel (b) of Figure 15, with the following values of the parameters: $\omega_N = 1454 \text{ cm}^{-1}$, $\Delta = 63 \text{ cm}^{-1}$, $g = 65 \text{ meV}$ [22], $\omega_{CT} = 0.94 \text{ eV}$ at room T [19], shifted at about 1.05 eV in the low-temperature phase [50]. The green dashed line shows the linear dependence of $a_g\nu_4$ frequency from ρ in the absence of e-mv coupling. The dots in panel (b) of the Figure correspond to the experimental frequencies above and below the phase transition shown in panel (a). The obtained estimates of ρ , 0.40 and 0.43 respectively, are rough, at the light the introduced approximations, but unambiguously show that the N-I borderline is not crossed at the phase transition.

At room temperature TMB-TCNQ crystallizes in the monoclinic system, $P2_1/n (C_{2h}^5)$, $Z = 2$, like TTF-CA. The stack dimerizes at the phase transition, and a minimum loss of symmetry implies the passage from a C_{2h} factor group to a either a C_s group, like TTF-CA [25], or to a C_2 group. Structural data of the low-temperature phase are hard to get, because the sample cracks or breaks, and the occurrence of the transition and its critical temperature are scarcely reproducible [47]. Also simple

grinding of the crystal may prevent the transition down to 77 K. Therefore a computational approach has been adopted to get some hint about the type of interaction triggering the transition and the associated mechanism [19]. In this particular case, a semi-empirical calculation, MOPAC16 with PM7 parametrization has been chosen, showing that the equilibrium geometry at 0 K belongs to the monoclinic $P2_1$ (C_2^2) space group. A comparison of the cell structure of the experimental high temperature phase and of the computed low temperature phase is given in Figure 16.

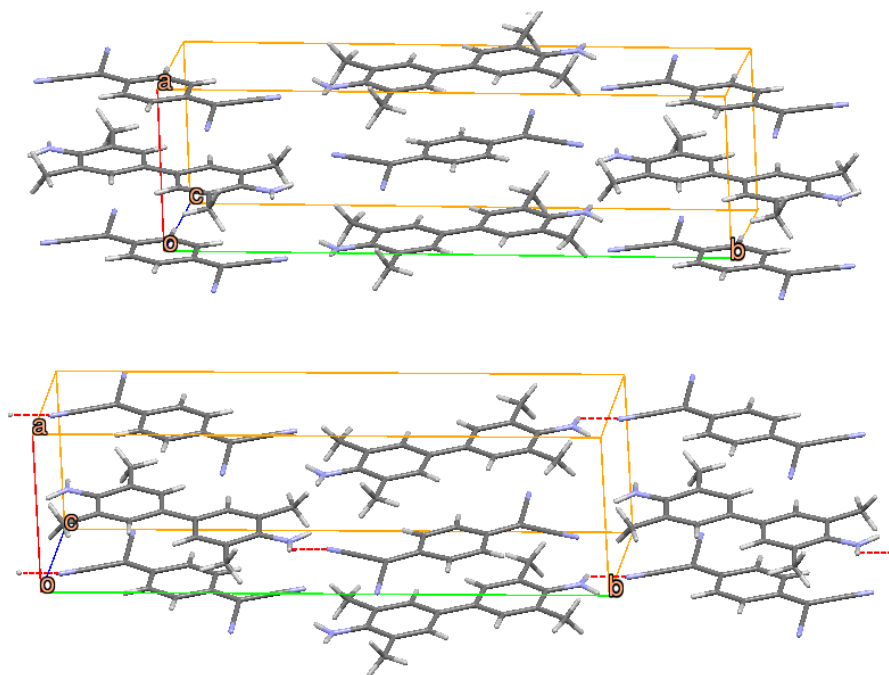


Figure 16. Crystal packing of TMB-TCNQ: top, experimental X-ray structure above the critical temperature. Bottom: calculated structure below the critical temperature. From [19].

According to the calculations, the symmetry breaking at the phase transition implies the loss of the inversion center, in agreement with the IR measurements, and of the glide plane. The a axis length increases and the c axis decreases, but overall the cell volume slightly *increases* in the low-temperature phase, which might well explain the crystal breaking. Moreover, the computed expansion and contraction along the a and c axes are consistent with experiment, indicating that the crystal breaking occurs precisely along these axes [47]. The arrangement of the DA dimers in the unit cell is anti-ferroelectric. The increase in the a stacking axis length at the transition is due to TMB molecular deformation and $H \cdots N$ interstack contacts between TMB and TCNQ. This is shown in Figure 16: In the low-temperature phase the apical NH_2 group of TMB deviates markedly from planarity, and establishes a closer contact with the Nitrogen of the TCNQ of the nearby stack (red dashed lines in the Figure; the $H \cdots N$ distance varies from 2.186 Å to 1.588 Å). It is therefore the TMB deformation and $H \cdots N$ contact that triggers the valence instability and the simultaneous stack dimerization.

Above the transition TMB-TCNQ is very similar to TTF-CA or DMeTTF-CA: Ionicity around 0.3, presence of dimerization mode(s) as detected by the combination bands. Yet by lowering the temperature the evolution of the three systems is different: TTF-CA undergoes a discontinuous NIT from 0.3 to 0.5, and DMTTF-CA displays an almost continuous ionicity change, accompanied by dimerization, but without crossing the N-I borderline. TMB-TCNQ instead has a first order transition with a discontinuous ionicity change, like TTF-CA, but again without crossing the N-I borderline. To give a rationale to these differences, one has to consider that by increasing the ionicity with lowering T , one reaches a multistability region [51], with a competition between a first order valence instability

driven by the 3D Madelung energy and a second order one-dimensional Peierls instability. At this point very weak intermolecular forces, all connected to the compressibility of the sample, i.e., to the (anisotropic) increase of the Madelung energy, may trigger the transition and drive the system towards one of the possible minima. The weak H \cdots N contacts in this case imply a cell expansion, so that the increase of ionicity due to the Madelung energy is very limited, and the N-I borderline is not crossed.

2.3. CIMEPD–DMEDCNQi

Whereas TMB–TCNQ is an example of a dramatic first-order transition with large hysteresis (~ 30 K) [19,46,47], 2-chloro-5-methyl-*p*-phenylenediamine–2,5-dimethyl-dicyanoquinonediimine (CIMEPD–DMEDCNQi) is on the opposite an unique case of a truly continuous NIT, accompanied by dimerization [20,52].

Figure 17 shows the temperature evolution of the CIMEPD–DMEDCNQi IR absorption spectrum with light polarization perpendicular to the stack axis. We immediately notice that the nearly isolated band around 1570 cm^{-1} , marked by an asterisk in the Figure, and due to DMEDCNQi C=C stretching $b_u \nu_{46}$, shows a remarkable frequency shift towards lower wavenumber. This mode is indeed one good charge sensitive vibration, exhibiting a ionization frequency shift of 61 cm^{-1} [53]. By using its frequency the observed red shift indicates a continuous ρ change from about 0.34 at 298 K to about 0.57 at 80 K.

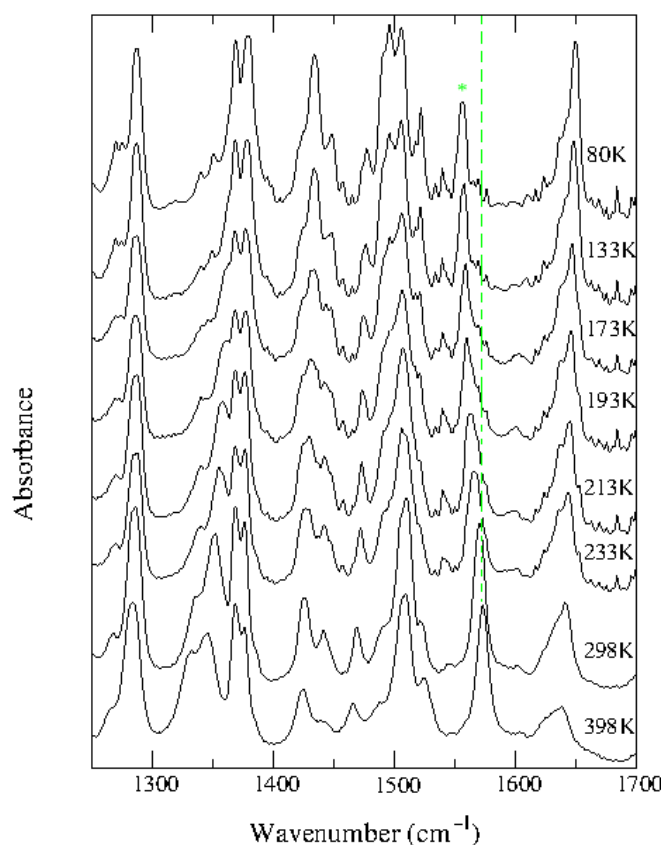


Figure 17. Temperature evolution of the CIMEPD–DMEDCNQi IR absorption spectra polarized perpendicular to the stack. The green asterisk and dashed line put in evidence the frequency change of the charge-sensitive DMEDCNQi C=C stretching $b_u \nu_{46}$. From [20].

In Figure 18 we report the temperature evolution of IR absorption spectra in the $800\text{--}1200$ and $1380\text{--}1800\text{ cm}^{-1}$, polarized along the stack. The e-mv induced bands due to totally symmetric modes are immediately recognized since they gain IR intensity by lowering the temperature, and also have their counterpart at the same frequency in the Raman spectra (not shown). The principal ones are

marked by a red asterisk in the Figure. We notice that at room temperature the e-mv induced bands are already developed to some extent. This residual IR intensity of the totally symmetric modes (about 10% of the low temperature value) puts in evidence that there is already some degree of stack distortion at 300 K. The residual IR intensity decreases further by increasing the temperature up to ~ 320 K.

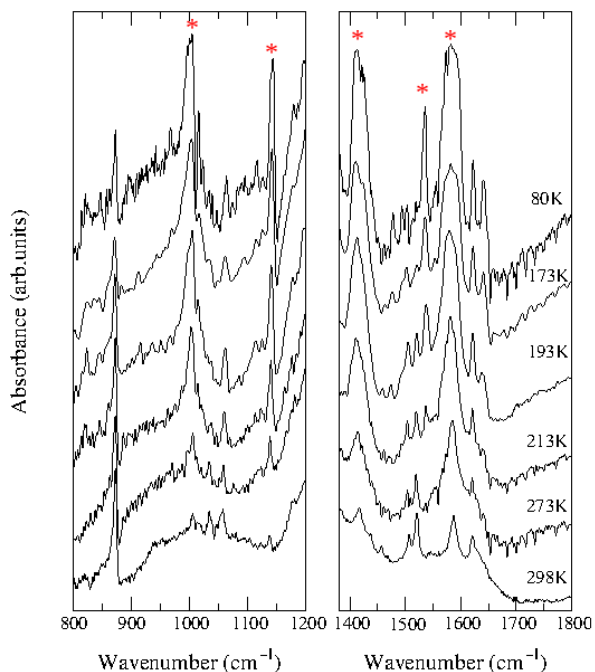


Figure 18. Temperature evolution of CIMEPD–DMEDCNQI IR absorption spectra polarized parallel to the stack. The red asterisks evidence the main e-mv induced bands. From [20].

The detailed evolution of the intensity enhancement of the e-mv induced bands has been followed picking up the bands around 1006 , 1417 and 1587 cm^{-1} , corresponding to the DMEDCNQI $a_g \nu_{13}, \nu_7, \nu_5$ modes [20]. Such T evolution of the e-mv induced bands, with normalization to the 80 K value, is compared with the corresponding evolution of ρ in Figure 19. The ionicity changes continuously with T , and the intensity of the e-mv induced IR bands, which is related to stack distortion, has the same S-shape as the ρ variation. The stack is already dimerized to some extent at room temperature, when $\rho = 0.34$. The point of maximum slope occurs in both cases around 220 K (violet dotted line in the top panel of Figure 19), whereas the conventional borderline of $\rho = 0.5$ occurs at 200 K. If ρ changes continuously the N-I borderline is ill-defined, but in any case the dimerization has started when the compound is still well into the neutral phase. Thus the dimerization represents the order parameter of transition, and the driving force appears to be the e-ph coupling. Since the ρ variation does not imply a symmetry change, we can equate the NI interface to the gas-liquid one, where we have a critical point beyond which there is no phase boundary. Then for CIMEPD–DMEDCNQI the data suggest that we are beyond the critical point: the interface is continuous and ρ is not an order parameter.

In ms CT crystals the position of the critical point for the passage from a discontinuous to a continuous NI interface depends on the ratio of the Madelung energy to the CT integral t_{DA} [12,13]. Structural investigations [52] have shown that indeed in CIMEPD–DMEDCNQI the interplanar D–A distance is shorter than in TTF–CA (3.13 Å vs 3.7 Å at room T) so t_{DA} is expected to be larger. On the other hand, CIMEPD–DMEDCNQI X-ray analysis at 150 K have also shown, rather surprisingly, that there is no symmetry lowering with respect to the 300 K structure. Both belongs to the triclinic $P\bar{1}$ (C_i) space group, and each of the two components of the complex is located on a special position possessing crystallographic C_i symmetry [54]. The CIMEPD molecule is not centrosymmetric, and the chlorine atom and methyl group of the CIMEPD are disordered with 50:50 occupancy at each site. Lowering the

temperature only reduces the cell volume, from 389.97 to 378.47 Å³, thus increasing the Madelung energy, but without establishing long-range stack dimerization. The apparent contradiction with the indications coming from IR spectra polarized parallel to the stack (Figure 18) can be solved by taking into account the presence of disorder [54]. Indeed CIMEPD is a polar molecule, with a dipole moment between 2.9 and 3.1 D oriented from Cl to Me. The polar CIMEPD occupy the C_i site with 50:50 different orientation on average, and generates disordered sites energies. As a consequence cooling increases the ionicity ρ , but disorder suppresses the Peierls instability and breaks inversion symmetry locally. As a consequence, the dimerization transition has to be classified as a disorder-to-order rather than a displacive one, and the order achieved at lowest temperature is in any case partial, as evidenced by the relatively low intensity of the e-mv induced bands. In such a kind of phase transition one does not expect the presence of soft modes, and no evidence has been found.

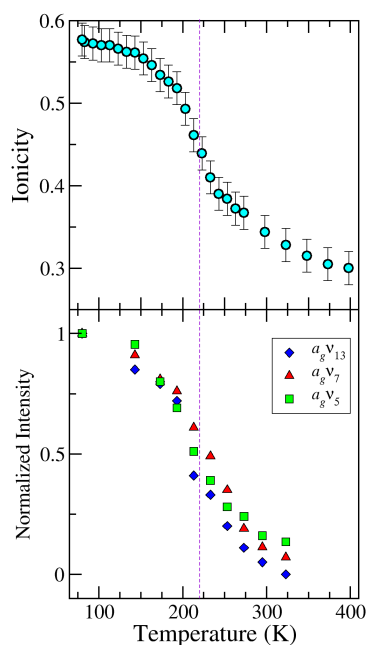


Figure 19. Top panel: Temperature evolution of the degree of CIMEPD–DMeDCNQI ionicity, estimated from the frequency of the DMeDCNQI $b_u\nu_{46}$ mode. Bottom panel: the corresponding change in the intensity of the e-mv induced bands, normalized to the low-temperature value. The violet dotted line signals the temperature of maximum slope of the two curves. Adapted from [20].

3. Pressure induced NIT

In their seminal paper [3] Torrance et al. claimed to have found ten CT systems undergoing NIT upon applying pressure through a diamond anvil cell (DAC). Subsequent studies have confirmed the reported critical pressure only in the case of TTF–CA: perylene–TCNE did not show evidence of NIT [55], the color change of DBTTF–TCNQ was associated to stack dimerization, before the crossing of the N–I interface [56], whereas for TTF–25Cl₂BQ such crossing occurs at pressure higher than that of the color change [57]. As a matter of fact, the critical pressure reported in [3] was actually the pressure of the visually monitored color change of the sample upon increasing pressure. However this color change may be simply due to the pressure shift of the relevant $\pi^* \leftarrow \pi$ transition of the D or A aromatic molecule [55]. Six out of the ten CT crystals originally reported have not been investigated any further, but other systems have since then added to the list, as detailed in Table 2.

Table 2. Pressure induced Neutral-Ionic transitions (ambient temperature)

System ^a	p _{NI} ^b (GPa)	Δρ Jump	ρ(p) Range	Ref.
TTF-CA	0.86–1.24	0.2	0.2–0.8	[58]
TTF-2,5Cl ₂ BQ	3.8	0	0.2–0.8	[57]
TTF-2,3,5Cl ₃ BQ	0.6–2.5	0.2	0.3–0.8	[59]
TTF-IA	1.9–2.2	0.1	0.0–0.6	[60]
TTF-DMeDCNQI	1.0	0.8	0.8	[61]
DMeTTF-CA	0.7–1.2	0.2	?	[62]
DMeTTF-BA	1.2	?	?	[14]
ClMePD-DMeDCNQI	0.75	0	0.4–0.7	[63]
DBTTF-TCNQ	1.1	0.1	0.3–0.4	[56]
BEDT-TTF-ClMeTCNQ	0.8–1.2	0.2 ?	0.3–1.0	[64]
TMB-TCNQ	0.49–2.7	?	?	[65]

^a TTF: tetrathiafulvalene; CA: chloranil; 2,5Cl₂BQ: 2,5-dichloro-*p*-benzoquinone; 2,3,5-trichloro-4-bromo-*p*-benzoquinone; IA: iodanil; DMeDCNQI: 2,5-dimethyl-dicyanoquinonediimine; DMeTTF: 4,4'-dimethyl-TTF; BA: bromanil; ClMePD: 2-chloro-5-methyl-*p*-phenyldiamine; DBTTF: dibenzo-tetrathiafulvalene; TCNQ: tetracyanoquinodimethane; BEDT-TTF: bis(ethylenedithio)tetrathiafulvalene; ClMeTCNQ: 2-chloro-5-methyl-TCNQ; TMB: 3,3',5,5'-tetramethylbenzidine. ^b When present, the *p* interval indicates a sort of intermediate regime.

Table 2 shows that the systems undergoing pressure-induced NIT are more numerous than those exhibiting temperature-induced NIT (Table 1). The reason is that by pressure one can easily reduce the volume (hence increase the Madelung energy) beyond that achievable at 0 K. On the other hand, Table 2 presents several question marks reflecting incompleteness of the collected data. The reason is twofold. First, making accurate measurements of single crystals inside the DAC is not easy, and most of the measurements have been indeed done on powdered samples. Furthermore, pressure homogeneity and precise control of pressure steps is difficult, the quality of optical and X-ray data is reduced, etc. Second, the interest may have been focused on specific aspects, like for instance the achievement of a quantum phase transition [14], for which a precise determination of parameters like ionicity or dimerization amplitude is not essential. One feature which appears to be common to several pressure-induced NIT is the presence of a sort of intermediate regime between the initial and the final phase. In several examples this intermediate regime is characterized by the simultaneous presence of two species of different ionicity.

As an example of a double ionicity intermediate regime we report in Figure 20 the well studied case of TTF-CA [58]. The panel (a) reports the pressure evolution of the IR spectra polarized perpendicular to the stack axis in the spectral region of C=O antisymmetric stretching. The behavior under pressure is quite different from the one on lowering the temperature, as evidenced from the comparison with the panel (a) of Figure 1: In the interval 0.85–1.10 GPa the C=O stretching band splits (continuous lines in the Figure), indicating the presence of differently charged species. It seems that the intermediate phase is not the paraelectric phase described in [28], since domains of different ionicity have comparable concentrations, and well defined ionicity. Therefore it is difficult to imagine that the phase between 0.86 and 1.24 GPa is a dynamic phase, characterized by the LR-CT, but rather a *statically disordered* mixed phase, defined by randomly oriented *polar* domains of different ionicity, which gradually polarize evolving towards the ordered ferroelectric phase above 1.24 GPa. In this scenario LR-CT excitations, which are thermally accessible at room temperature [51], are invoked to explain anomalies in conductivity [66] and in dielectric response [67] observed just *before* 0.86 GPa.

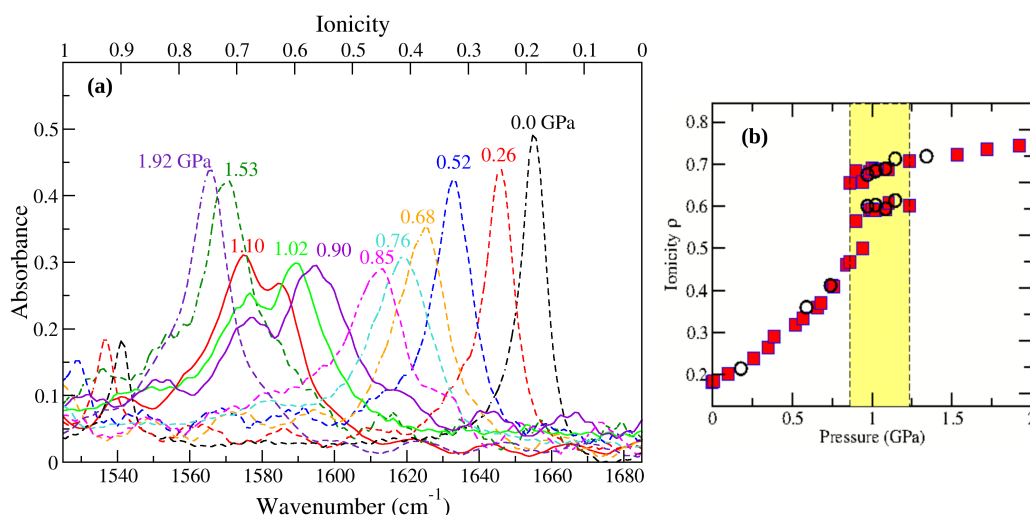


Figure 20. (a) Pressure evolution of TTF-CA IR spectra polarized perpendicular to the stack axis in the C=O antisymmetric stretching spectral region. (b) TTF-CA ionicity change under pressure. The yellow region marks the pressure range of the intermediate regime. Adapted from [58].

We have chosen TTF-CA to illustrate the intermediate regime observed in pressure-induced NIT (Table 2), since this is one of the few cases in which accurate measurements, including pressure uniformity checks, have been performed on single crystals. Yet, the above sketched scenario has to be considered highly speculative, and additional measurements and modeling would be required to confirm or disprove it. The same applies to the other CT crystals listed in Table 2, and to lesser extent to the Tp phase diagrams proposed for TTF-CA [28], for the DMeTTF-haloquinone series [14,18] and BEDT-TTF-ClMeTCNQ [68]. For these reasons we shall not try to give here a more detailed and comprehensive description of the pressure-induced NIT.

4. Beyond the NIT: Exploring the Phase Space of ms CT Crystals

At ambient conditions, essentially four different classes of 1:1 ms CT crystals have been structurally identified: (i) Neutral regular stack, with dimerization amplitude $\delta = 0$ and ionicity $\rho \lesssim 0.5$; (ii) Neutral dimerized stack, with $\delta \neq 0$ and $\rho \lesssim 0.5$; (iii) Ionic dimerized stack, with $\delta \neq 0$ and $\rho \gtrsim 0.5$; (iv) Ionic regular stacks, with $\delta = 0$ and $\rho \gtrsim 0.5$. The latter class exist only at finite temperatures, as ionic regular stacks are intrinsically unstable towards dimerization [7]. Although several aspects of NIT, particularly the p -induced ones, still await full understanding, researchers interests have slowly drifted towards more application-oriented issues [9]. In particular, complexes belonging to the TTF-haloquinone family, TTF-CA, TTF-BrCl₃BQ and TTF-BA (BA: Bromanil) have been shown to display *electronic* ferroelectricity in their low-temperature, ionic dimerized phase [69,70]. In addition, a recent theoretical paper suggested that Neutral regular stack CT crystals might be good semiconductors with balanced electron and hole transport [71], and indeed the well known DBTTF-TCNQ (cf. Table 2), among others, has been found to exhibit such a property, although with limited mobility values [72]. Mainly for these reasons, several studies have appeared aimed at exploring the phase space of ms CT crystals at ambient conditions [73–77], tuning the band gap, and at the same time moving towards the N-I borderline, where the stack dimerizes and becomes potentially ferroelectric.

In the present context, the series of 1:1 CT crystals of perylene with TCNQF_x (Table 3) is particularly interesting [75,76]. In this series the HOMO-LUMO gap and degree of CT are tuned by increasing the electron affinity of the Acceptor by the number of fluorine atoms, while keeping the Donor constant. The crystals are not isomorphous, but the type of HOMO-LUMO overlap is the same along the series, so the hopping integral can be considered approximately constant, between about 0.25 and 0.35 eV [76]. In these conditions the optical gap and the ionicity change monotonically with

TCNQF_x electron affinity. The stack is regular, and the degree of CT ρ increases from about 0.01 to 0.29, the latter value being higher than that of TTF-CA at ambient condition. And indeed Per-TCNQF₄ is near to the N-I borderline, and according to Torrance et al. undergoes NIT at about 1.1 GPa [3]. We have verified that Per-TCNQF₄ does not undergo NIT by lowering T to 77 K. We did not try lower temperature since from 300 to 77 K there is virtually no change in the frequency of the charge sensitive modes, i.e., no increase in ρ by lowering T , as it happens for TTF-CA (Figure 1a). Clearly, the thermal contraction of Per-TCNQF₄ is relatively small, so there is not NIT at ambient pressure.

Table 3. Space group, degree of CT ρ and peak/onset of the CT transition in 1:1 perylene-TCNQF_x.

System ^a	Space Group	ρ	ω_{CT} (eV)	Ref.
Per-TCNQ	$P2_1/c$ (C_{2h}^5)	0.01	1.34, onset 1.05	[76]
Per-TCNQF	$P2_1/c$ (C_{2h}^5)	0.08	–	[75]
Per-TCNQF ₂	$P2_1/n$ (C_{2h}^5)	0.13	onset 0.88	[76]
Per-TCNQF ₄	$P\bar{1}$ (C_1^1)	0.29	0.98, onset 0.71	[76]

^a Per: perylene; TCNQ: tetracyanoquinodimethane; TCNQF: 2-fluoro-tetracyanoquinodimethane; TCNQF₂: 2,5-difluoro-tetracyanoquinodimethane; TCNQF₄: tetrafluoro-tetracyanoquinodimethane.

With the aim of spanning a larger range of ρ , we have decided to combine 3,3',5,5'-tetramethylbenzidine (TMB), a Donor stronger than perylene, with CA, BA, TCNQF₂ and TCNQF₄. The CT crystal TMB-TCNQ is already characterized, and is close to the N-I borderline (see Section 2.2). Table 4 reports some significant preliminary data. From the Table it is seen that at ambient condition ρ increases monotonically from 0.14 to 0.89 with the increase of the Acceptor electron affinity. Therefore we cross the N-I borderline by chemical substitution. TMB-CA and TMB-BA are isomorphous, and the stack is regular. By lowering T the ionicity increases slightly, but we do not observe phase transitions down to 10 K. TMB-TCNQ stack is regular at room temperature, then around 200 K has a valence instability with $\Delta\rho \sim 0.1$ and stack dimerization [19]. TMB-TCNQF₂, beyond the N-I borderline, crystallizes in the same space group as that hypothesized for TMB-TCNQ low-temperature phase, with two dimerized stack per cell, arranged antiferromagnetically. Finally, TMB-TCNQF₄ is well on the ionic side, with contrasting evidences about dimerization, since the group is centrosymmetric, but IR spectra polarized parallel to stack are characterized by the appearance of the e-mv induced bands typical of dimerization. The situation closely resembles that of tetramethyl-*p*-phenyldiamine-TCNQ (TMPD-TCNQ) [78], and further studies, also as a function of T , are in progress to clarify the issue.

Table 4. Space group, degree of CT ρ and peak/onset of the CT transition in 1:1 TMB-Acceptor.

System ^a	Space Group	ρ	ω_{CT} (eV)	Ref.
TMB-CA	$C2/m$ (C_{2h}^3)	0.14	onset 0.67	This work
TMB-BA	$C2/m$ (C_{2h}^3)	0.16	onset 0.61	This work
TMB-TCNQ	$P2_1/n$ (C_{2h}^5)	0.29	0.94, onset 0.46	[19]
TMB-TCNQF ₂	$P2_1$ (C_2^2)	0.65	onset 0.57	This work
TMB-TCNQF ₄	$C2/m$ (C_{2h}^3)	0.89	onset 0.47	This work

^a TMB: 3,3',5,5'-tetramethylbenzidine; CA: chloranil; BA: bromanil; TCNQ: tetra- cyanoquinodimethane; TCNQF: 2-fluoro-tetracyanoquinodimethane; TCNQF₂: 2,5-difluoro- tetracyanoquinodimethane; TCNQF₄: tetrafluoro-tetracyanoquinodimethane.

These new series of ms CT crystals, together with the other already known [7], fit the general picture that can be drawn on the basis of a modified 1D Hubbard model, including e-mv and e-ph coupling [39]. Neutral stacks are regular, but there is a Peierls transition to dimerized stack as ρ increases, and indeed systems with ρ between 0.3–0.4 and 0.8–0.9 are dimerized at ambient conditions.

More ionic crystals, like TTF–BA, can be regular at room temperature, but the ground state is in any case dimerized due the Peierls unconditional instability. Ferroelectricity requires dimerized stacks, hence appreciable degree of CT. On the other hand, mobilities are expected to improve with large hopping integrals which favor electron delocalization, and the stack has to remain regular, hence well on the neutral side. One might then think to be able to design and synthesize CT crystals with the sought features by properly choosing the DA pair. However, further exploration of the ms CT phase space is required in order to address and solve the numerous problems still remaining on the way of achieving such an ambitious goal.

5. Summary

After 35 years since its discovery [4], a reasonable general understanding of the temperature induced NIT and of the associated phenomena has been reached. The initial idea of the Madelung energy as the only driving-force of the phase transition soon had to be integrated with the role of the e-ph coupling, which yields the stack dimerization through the Peierls mechanism. And many of the anomalies associated with the NIT can be accounted for in terms of the presence of soft phonons, i.e., phonons strongly coupled to the 1D electronic system and hence anharmonic (see Section 2.1.3 and [39]). On the other hand, the role the so-called LR-CT in these phenomena cannot be completely excluded, unless one makes use the “Occam’s razor” principle. These exotic objects are likely at the basis of dynamic anomalies as the nonlinear electric transport [35], and from this point of view a non-phenomenological model of LR-CT would be highly desirable.

Although electron-electron and electron-phonon are the main interactions involved in the NIT [39], some ingredients are still missing from the general picture. As a matter of fact, we still cannot answer the apparently naive question of why the number of systems undergoing the NIT is still so limited (Table 1). As discussed in Section 2.2, an explanation of this fact can be given by considering that by increasing the ionicity with lowering T , one reaches a multistability region [51], with a competition between a first order valence instability driven by the 3D Madelung energy and a second order 1D Peierls instability. At this point very weak intermolecular forces, like hydrogen [27] or halogen bonding, or other forces connected to the sample compressibility, may trigger the transition and drive the system towards one of the possible minima. We believe that such a kind of complex scenario explains why NIT are so rare, and why the occurrence and the actual type of phase transition is so difficult to predict. We cite just as one example the case of Per–TCNQF₄ (Table 3), which at room temperature looks quite similar to TTF–CA, but does not come closer to the N-I borderline by lowering T to 77 K.

The same kind of weak interactions are involved in another issue, i.e., the possible occurrence of different polymorphs. In fact, the physics of CT crystals is based on CT interaction, which is dominant and highly directional, giving rise to stack arrangement and low-dimensional electronic structure. Yet, the formation of stacks and their packing is determined by more subtle, sometimes difficult to control, interactions. Letting aside the possibility of D:A ratios different from 1:1 [73], there are cases of a DA pair growing in either segregated or mixed stack, like tetramethyl-tetraselenofulvalene–TCNQ [79,80], or of the growth of different polymorphs with ms motif, as DBTTF–TCNQ [81,82]. Even the prototypical TTF–CA has at least two polymorphs, with quite different electronic properties [10,83]. Finally, if one tries to tune the degree of CT by changing the Acceptor electron affinity, like in the series of Table 4, but with TTF as Donor, finds that TTF–CA is ms, $\rho = 0.2$, TTF–BA is ms, but fully ionic [11], whereas the compounds with TCNQF_x are all segregated stack: TTF–TCNQ, the well known metal with $\rho = 0.59$ [84], and TTF–TCNQF₂ and TTF–TCNQF₄ both fully ionic Mott insulators [85,86]. From these few examples one realizes that the factor controlling the packing of CT crystals are so far not well understood nor controlled. HOMO-LUMO overlap, molecular shape and flexibility, hydrogen and halogen-bonding, and Madelung energy are all factors contributing to the resulting structure. Extending the exploration of the phase space of CT crystal will hopefully shed light on these factors, opening the way to the methods of crystal engineering to effectively control the physical properties of CT crystals.

Acknowledgments: Research supported in part by the Parma University local Research Funding program (FIL). Funds for covering the costs to publish in open access have not been received. We thank G. D'Avino, A. Painelli, C. Rizzoli and Z. G. Soos for enlightening discussions.

Author Contributions: Alberto Girlando and Matteo Masino conceived and designed the experiments; Matteo Masino and in part Nicola Castagnetti performed the experiments and analyzed the data; Alberto Girlando wrote the paper.

Conflicts of Interest: The authors declare no conflict of interest. The founding sponsors had no role in the design of the study; in the collection, analyses, or interpretation of data; in the writing of the manuscript, and in the decision to publish the results.

Abbreviations

The following abbreviations are used in this manuscript:

CT	charge-transfer
D	π -electron Donor
A	π -electron Acceptor
ms	mixed stack
NIT	Neutral-Ionic transition
N	Neutral or quasi-Neutral ground state
I	Ionic or quasi-Ionic ground state
3D	three-dimensional
1D	one-dimensional
CO	Charge Order
IR	infrared
e-mv	electron-molecular vibration
e-ph	electron-(lattice) phonon
QHLD	Quasi-Harmonic Lattice Dynamics
LR-CT	Lattice-Relaxed exciton strings
NIDW	Neutral-Ionic Domain Walls
DAC	diamond anvil cell

References

1. Soos, Z.G. Theory of π -molecular charge-transfer crystals. *Ann. Rev. Phys. Chem.* **1974**, *25*, 121–153.
2. McConnell, H.M.; Hoffman, B.M.; Metzger, R.M. Charge transfer in molecular crystals. *Proc. Natl. Acad. Sci. USA* **1965**, *53*, 46–50.
3. Torrance, J.B.; Vazquez, J.E.; Mayerle, J.J.; Lee, V.Y. Discovery of a neutral-to-ionic phase transition in organic materials. *Phys. Rev. Lett.* **1981**, *46*, 253–257.
4. Torrance, J.B.; Girlando, A.; Mayerle, J.J.; Crowley, J.I.; Lee, V.Y.; Batail, P.; LaPlaca, S.J. Anomalous nature of neutral-to-ionic phase transition in tetrathiafulvalene-chloranil. *Phys. Rev. Lett.* **1981**, *47*, 1747–1750.
5. Koshihara, S.; Tokura, Y.; Mitani, T.; Saito, G.; Koda, T. Photoinduced valence instability in the organic molecular compound tetrathiafulvalene- p-choranil (TTF-CA). *Phys. Rev. B* **1990**, *42*, 6853–6856.
6. Nad, F.; Monceau, P.; Fabre, J.M. Low frequency dielectric permittivity of quasi-one-dimensional conductor (TMTTF)₂Br. *Eur. Phys. J. B* **1998**, *3*, 301–306.
7. Girlando, A.; Painelli, A.; Bewick, S.A.; Soos, Z.G. Charge fluctuations and electron-phonon coupling in organic charge-transfer salts with neutral-ionic and Peierls transitions. *Synth. Met.* **2004**, *141*, 129–138.
8. Horiuchi S.; Kumai R.; Okimoto, Y.; Tokura Y. Chemical approach to neutral-ionic valence instability, quantum phase transitions and relaxor ferroelectricity in organic charge-transfer complexes. *Chem. Phys.* **2006**, *325*, 78–91.
9. Horiuchi S.; Hasegawa, T.; Tokura Y. Molecular Donor-Acceptor compounds as prospective organic electronics materials. *J. Phys. Soc. Japan* **2006**, *75*, 051016.
10. Girlando, A.; Marzola, F.; Pecile, C.; Torrance, J.B. Vibrational spectroscopy of mixed stack organic semiconductors: Neutral and ionic phases of tetrathiafulvalene-chloranil (TTF-CA). *J. Chem. Phys.* **1983**, *79*, 1075–1085.

11. Girlando, A.; Pecile, C.; Torrance, J.B. A key to understanding ionic mixed stack organic solids: Tetrathiafulvalene-bromanil. *Solid State Commun.* **1985**, *54*, 753–759.
12. Girlando, A.; Painelli, A. Regular-dimerized stack and neutral-ionic interfaces in mixed-stack organic charge-transfer crystals. *Phys. Rev. B* **1986**, *34*, 2131–2139.
13. Painelli, A.; Girlando, A. Zero-temperature phase diagram of mixed-stack charge-transfer crystals. *Phys. Rev. B* **1988**, *37*, 5748–5760 and *Phys. Rev. B* **1989**, *39*, 9663 (Erratum).
14. Horiuchi, S.; Okimoto, Y.; Kumai, R.; Tokura, Y. Quantum phase transition in organic charge-transfer complexes. *Science* **2003**, *299*, 229–232.
15. Tokura Y.; Kaneko, Y.; Okamoto, H.; Tanuma, S.; Koda, T.; Mitani, T.; Saito, G. Spectroscopic study of the neutral-to-ionic phase transition in TTF-Chloranil. *Mol. Cryst. Liq. Cryst.* **1985**, *125*, 71–80.
16. Horiuchi, S.; Okimoto, Y.; Kumai, R.; Tokura, Y. Anomalous charge fluctuations near a ferroelectric transition in an organic charge-transfer complex. *J. Phys. Soc. Japan* **2000**, *69*, 1302–1305.
17. Ranzieri, P.; Masino, M.; Girlando, A.; Lemée-Cailleau, M.H. Temperature-induced valence and structural instability in DMTTF-CA: Single crystal Raman and infrared measurements. *Phys. Rev. B* **2007**, *76*, 134115.
18. Horiuchi, S.; Okimoto, Y.; Kumai, R.; Tokura, Y. Ferroelectric valence transition and phase diagram of a series of charge-transfer complexes of 4,4'-dimethyltetrathiafulvalene and tetrahalo-*p*-benzoquinones. *J. Am. Chem. Soc.* **2001**, *123*, 665–670.
19. Castagnetti, N.; Kociok-Köhn, G.; Da Como, E.; Girlando, A. Temperature-induced valence instability in the charge-transfer crystal TMB-TCNQ. *Phys. Rev. B* **2017**, *95*, 024101.
20. Masino, M.; Girlando, A.; Farina, L.; Brillante, A. A new type of neutral-ionic interface in mixed stack organic charge transfer crystals: Temperature induced ionicity change in CIMEPD-DMeDCNQI. *Phys. Chem. Chem. Phys.* **2001**, *3*, 1904–1910.
21. Painelli, A.; Girlando, A. Electron-molecular vibration (e-mv) coupling in charge transfer compounds and its consequences on the optical spectra: A theoretical framework. *J. Chem. Phys.* **1986**, *84*, 5655–5671.
22. Pecile, C.; Painelli, A.; Girlando, A. Studies of organic semiconductors for 40 years—V. *Mol. Cryst. Liq. Cryst.* **1989**, *171*, 69–87.
23. Girlando, A.; Bozio, R.; Pecile, C.; Torrance, J.B. Discovery of vibronic effects in the Raman spectra of mixed-stack charge-transfer crystals. *Phys. Rev. B* **1982**, *26*, 2306–2309.
24. Ranzieri, P.; Masino, M.; Girlando, A. Charge-sensitive vibrations in *p*-chloranil: The strange case of the C=C antisymmetric stretching. *J. Phys. Chem. B* **2007**, *111*, 12844–12848.
25. Le Cointe, M.; Lemée-Cailleau, M.H.; Cailleau, H.; Toudic, B.; Toupet, L.; Heger, G.; Moussa, F.; Schweiss, P.; Kraft, K.H.; Karl, N. Symmetry breaking and structural changes at the neutral-to-ionic transition in tetrathiafulvalene-*p*-chloranil. *Phys. Rev. B* **1995**, *51*, 3374–3386.
26. Collet, E.; Buron-Le Cointe, M.; Lemée-Cailleau, M.H.; Cailleau, H.; Toupet, L.; Meven, M.; Mattauch, S.; Heger, G.; Karl, N. Structural evidence of ferrielectric neutral-ionic layered ordering in 2,6-dimethyltetrathiafulvalene-*p*-chloranil. *Phys. Rev. B* **2001**, *63*, 054105.
27. Oison, V.; Katan, C.; Koenig, C. Intramolecular electronic redistribution coupled to hydrogen bonding: An important mechanism for the “Neutral-to-Ionic” transition. *J. Phys. Chem. A* **2001**, *105*, 4300–4307.
28. Lemée-Cailleau, M.H.; Le Cointe, M.; Cailleau, H.; Luty, T.; Moussa, F.; Roos, J.; Brinkmann, D.; Toudic, B.; Ayache, C.; Karl, N. Thermodynamics of the Neutral-to-Ionic transition as condensation and crystallization of charge-transfer excitations. *Phys. Rev. Lett.* **1997**, *79*, 1690–1693.
29. Moreac, A.; Girard, A.; Delugeard Y.; Marqueton, Y. The neutral-to-ionic phase transition of TTF-CA: A Raman and infrared study versus temperature at atmospheric pressure. *J. Phys. Condens. Matter* **1996**, *8*, 3553–3567.
30. Masino, M.; Girlando, A.; Soos, Z.G. Evidence for a soft mode in the temperature induced neutral-ionic transition of TTF-CA. *Chem. Phys. Lett.* **2003**, *369*, 428–433.
31. Masino, M.; Girlando, A.; Brillante, A.; Della Valle, R.G.; Venuti, E.; Drichko, N.; Dressel, M. Lattice dynamics of TTF-CA across the neutral-ionic transition *Chem. Phys.* **2006**, *325*, 71–77.
32. Girlando, A.; Masino, M.; Painelli, A.; Drichko, N.; Dressel, M.; Brillante, A.; Della Valle, R.G.; Venuti, E. Direct evidence of overdamped Peierls-coupled modes in temperature-induced phase transition in tetrathiafulvalene-chloranil. *Phys. Rev. B* **2008**, *78*, 045103.
33. Soos, Z.G.; Bewick, S.A.; Peri, A.; Painelli, A. Dielectric response of modified Hubbard models with neutral-ionic and Peierls transitions. *J. Chem. Phys.* **2004**, *120*, 6712–6720.

34. Masino, M.; Girlando, A. Peierls modes in the ionic phase of TTF-CA. Internal Report 2010 MG10-1 available upon request.
35. Tokura, Y.; Okamoto, H.; Koda, T.; Mitani, T.; Saito, G. Nonlinear electric transport and switching phenomenon in the mixed-stack charge-transfer crystal tetrathiafulvalene-*p*-chloranil. *Phys. Rev. B* **1988**, *38*, 2215–2218.
36. Heeger, A.J.; Kivelson, S.; Schrieffer, J.R.; Su, W.P. Solitons in conducting polymers. *Rev. Mod. Phys.* **1988**, *60*, 781–850.
37. Mitani, T.; Saito, G.; Tokura, Y.; Koda, T. Soliton Formation at the Neutral-to-Ionic Phase Transition in the Mixed-Stack Charge-Transfer Crystal Tetrathiafulvalene-*p*-Chloranil. *Phys. Rev. Lett.* **1984**, *53*, 842–845.
38. Nagaosa, N. Domain wall picture of the Neutral-Ionic transition in TTF-Chloranil. *Solid State Commun.* **1986**, *57*, 179–183.
39. D'Avino, G.; Soos, Z.G.; Painelli, A. Modeling the Neutral-Ionic transition with correlated electrons coupled to soft lattices and molecules. *Crystals* **2017**, *7*, 144.
40. Buron-Le Cointe, M.; Lemée-Cailleau, M.H.; Cailleau, H.; Ravy, S.; Bézar, J.F.; Rouzière, S.; Elkaïm, E.; Collet, E. One-dimensional fluctuating nanodomains in the charge-transfer molecular system TTF-CA and their first-order crystallization. *Phys. Rev. Lett.* **2006**, *96*, 205503.
41. Collet, E.; Lemée-Cailleau, M.H.; Buron-Le Cointe, M.; Cailleau, H.; Ravy, S.; Luty, T.; Bézar, J.F.; Czarnecki, P.; Karl, N. Direct evidence of lattice-relaxed charge transfer exciton strings. *Europhys. Lett.* **2002**, *57*, 67–73.
42. D'Avino, G.; Girlando, A.; Painelli, A.; Lemée-Cailleau, M.H.; Soos, Z.G. Anomalous dispersion of the optical phonons at the Neutral-Ionic transition: Evidence from diffuse X-ray scattering. *Phys. Rev. Lett.* **2007**, *99*, 156407.
43. Kohn, W. Image of the Fermi surface in the vibration spectrum of a metal. *Phys. Rev. Lett.* **1959**, *2*, 393–394.
44. Kendziora, C.A.; Sergienko, I.A.; Jin, R.; He, J.; Keppens, V.; Sales, B.C.; Mandrus, D. Goldstone-Mode phonon dynamics in the pyrochlore Cd₂Re₂O₇. *Phys. Rev. Lett.* **2005**, *95*, 125503.
45. D'Avino, G.; Masino, M.; Girlando, A.; Painelli, A. Correlated electrons in soft lattices: Raman scattering evidence of the nonequilibrium dielectric divergence at the neutral-ionic phase transition. *Phys. Rev. B* **2011**, *83*, 161105(R).
46. Iwasa, Y.; Koda, T.; Tokura, Y.; Kobayashi, A.; Iwasawa, N.; Saito, G. Temperature-induced neutral-ionic transition in tetramethylbenzidine-tetracyanoquinodimethane (TMB-TCNQ). *Phys. Rev. B* **1990**, *42*, 2374–2377.
47. Buron-LeCointe, M.; Lemée-Cailleau, M.H.; Cailleau, H.; Toudic, B.; Moréac, A.; Moussa, F.; Ayache, C.; Karl, N. Thermal hysteresis and mesoscopic phase coexistence around the neutral-ionic phase transition in TTF-CA and TMB-TCNQ. *Phys. Rev. B* **2003**, *68*, 064103.
48. Meneghetti, M.; Pecile, C. Charge-transfer organic crystals: Molecular vibrations and spectroscopic effects of electron-molecular vibration coupling of the strong electron acceptor TCNQF₄. *J. Chem. Phys.* **1986**, *84*, 4149–4162.
49. Hanfland, M.; Brillante, A.; Girlando, A.; Syassen, K. Raman study of the pressure induced neutral-to-ionic transition in tetrathiafulvalene-chloranil (TTF-CA). *Phys. Rev. B* **1988**, *38*, 1456–1461.
50. Iwasa, Y.; Soga, I.; Koda, T.; Tokura, Y.; Saito, G. Neutral-Ionic transition in TTF-Chloranil and TMB-TCNQ. *Synth. Met.* **1991**, *42*, 1827–1830.
51. Soos, Z.G.; Painelli, A. Metastable domains and potential energy surfaces in organic charge-transfer salts with neutral-ionic phase transitions. *Phys. Rev. B* **2007**, *75*, 155119.
52. Aoki, S.; Nakayama, T. Temperature-induced neutral-ionic transition in 2-chloro-5-methyl-*p*-phenylenediamine-2,5-dimethyl-dicyanoquinonediimine. *Phys. Rev. B* **1997**, *56*, R2893–R2896.
53. Lunardi, G.; Pecile, C. *N,N'*-dicyanoquinonediimines as a molecular constituent of organic conductors: Vibrational behavior and electron-molecular vibration coupling. *J. Chem. Phys.* **1991**, *95*, 6911–6923.
54. Bewick, S.A.; Pascal, R.A.; Ho, D.M.; Soos, Z.G.; Masino, M.; Girlando, A. Disorder in organic charge-transfer single crystals: Dipolar disorder in ClMePD-DMeDCNQI. *J. Chem. Phys.* **2005**, *122*, 024710.
55. Jurgensen, C.W.; Drickamer, H.G. High-pressure studies of the neutral-to-ionic transition in some organic charge-transfer solids. *Chem. Phys. Lett.* **1986**, *125*, 554–556.
56. Girlando, A.; Pecile, C.; Brillante, A.; Syassen, K. High-pressure optical studies of neutral-ionic phase transitions in organic charge-transfer crystals. *Synth. Met.* **1987**, *19*, 503–508.

57. Brillante, A.; Girlando, A. Pressure-driven phase transition in tetrathiafulvalene-2,5-dichloro-*p*-benzoquinone: Example of a continuous ionicity change. *Phys. Rev. B* **1992**, *45*, 7026–7030.
58. Masino, M.; Girlando, A.; Brillante, A. Intermediate regime in the pressure-induced neutral-ionic transition in tetrathiafulvalene-chloranil. *Phys. Rev. B* **2007**, *76*, 061114/1–061114/6.
59. Okamoto, H.; Koda, T.; Tokura, Y.; Mitani, T.; Saito, G. Pressure-induced neutral-to-ionic phase transition in organic charge-transfer crystals of tetrathiafulvalene-*p*-benzoquinone derivatives. *Phys. Rev. B* **1989**, *39*, 10693–10701.
60. Matsuzaki, S.; Hiejima, T.; Sano, M. Pressure-induced neutral-ionic phase transition of a tetrathiafulvalene-iodanil crystal. *Bull. Chem. Soc. Jpn.* **1991**, *65*, 2052–2057.
61. Basaki, S.; Matsuzaki, S. A new charge-transfer system for neutral-ionic transition: Tetrathiafulvalene-dimethyldicyanoquinonediimine. *Solid State Commun.* **1994**, *91*, 865–868.
62. Aoki, S.; Nakayama, T.; Miura, A. Neutral-ionic transition in dimethyl-TTF-chloranil. *Synth. Met.* **1995**, *70*, 1243–1244.
63. Farina, L.; Brillante, A.; Masino, M.; Girlando, A. Pressure-driven neutral-ionic transition in CIMEPD-DMeDCNQI. *Phys. Rev. B* **2001**, *64*, 144102.
64. Hasegawa, T.; Akutagawa, T.; Nakamura, T.; Mochida, T.; Kondo, R.; Kagoshima, S.; Iwasa, Y. Neutral-ionic phase transition of BEDT-TTF-CIME TCNQ under pressure. *Phys. Rev. B* **2001**, *64*, 085106.
65. Iwasa, Y.; Watanabe, N.; Koda, T.; Saito, G. Two-step neutral-ionic phase transition in organic charge-transfer compounds: Possible staging effects. *Phys. Rev. B* **1993**, *47*, 2920–2923.
66. Mitani, T.; Kaneko, Y.; Tanuma, S.; Tokura, Y.; Koda, T.; Saito, G. Electric conductivity and phase diagram of a mixed-stack charge-transfer crystal: Tetrathiafulvalene-*p*-chloranil. *Phys. Rev. B* **1987**, *35*, 427–429.
67. Okamoto, H.; Mitani, T.; Tokura, Y.; Koshihara, S.; Komatsu, T.; Iwasa, Y.; Koda, T.; Saito, G. Anomalous dielectric response in tetrathiafulvalene-*p*-chloranil as observed in temperature- and pressure-induced neutral-to-ionic phase transition. *Phys. Rev. B* **1991**, *43*, 8224–8232.
68. Lemée-Cailleau, M.H.; Collet, E.; Buron-Le Cointe, M.; Grach, N.; Ouladdiaf, B.; Moussa, F.; Hasegawa, T.; Takahashi, Y.; Roisnel, T.; Cailleau, H. Down to the quantum limit at the Neutral-to-Ionic phase transition of (BEDT-TTF)-(CIME-TCNQ): Symmetry analysis and phase diagram. *J. Phys. Chem. B* **2007**, *111*, 6167–6172.
69. Kagawa, F.; Horiuchi, S.; Tokunaga, M.; Fujioka, J.; Tokura, Y. Ferroelectricity in a one-dimensional organic quantum magnet. *Nat. Phys.* **2010**, *6*, 169–172.
70. Kobayashi, K.; Horiuchi, S.; Kumai, R.; Kagawa, F.; Murakami, Y.; Tokura, Y. Electronic ferroelectricity in a molecular crystal with large polarization directing antiparallel to ionic displacement. *Phys. Rev. Lett.* **2012**, *108*, 237601.
71. Zhu, L.Y.; Yi, Y.P.; Li, Y.; Kim, E.G.; Coropceanu, V.; Bredas, J.-L. Prediction of remarkable ambipolar charge-transport characteristics in organic mixed-stack charge-transfer crystals. *J. Am. Chem. Soc.* **2012**, *134*, 2340–2347.
72. Wu, H.-D.; Wang, F.-X.; Xiao, Y.; Pan, G.-B. Preparation and ambipolar transistor characteristics of co-crystal microrods of dibenzotetrathiafulvalene and tetracyanoquinodimethane. *J. Mater. Chem. C* **2013**, *1*, 2286–2289.
73. Vermeulen, D.; Zhu, L.Y.; Goetz, K.P.; Hu, P.; Day, C.S.; Jurchescu, O.D.; Coropceanu, V.; Kloc, C.; McNeil, L.E. Charge transport properties of Perylene-TCNQ crystals: The Effect of stoichiometry. *J. Phys. Chem. C* **2014**, *118*, 24688–24696.
74. Tsutsumi, J.; Matsuoka, S.; Inoue, S.; Minemawari, H.; Yamada, Y.; Hasegawa, T. N-type field-effect transistors based on layered crystalline donor-acceptor semiconductors with dialkylated benzothienobenzothiophenes as electron donors. *J. Mater. Chem. C* **2015**, *3*, 1976–1981.
75. Hu, P.; Du, K.; Wei, F.; Jiang, H.; Kloc, C. Crystal growth, HOMO-LUMO engineering, and charge transfer degree in Perylene-F_xTCNQ (x = 1, 2, 4) organic charge transfer binary compounds. *Cryst. Growth Des.* **2016**, *16*, 3019–3027.
76. Salzillo, D.; Masino, M.; Kociok-Köhn, G.; di Nuzzo, D.; Venuti, E.; Della Valle, R.G.; Vanossi, D.; Fontanesi, C.; Girlando, A.; Brillante, A.; et al. Structure, stoichiometry, and charge transfer in cocrystals of Perylene with TCNQ-F_x. *Cryst. Growth Des.* **2016**, *16*, 3028–3036.
77. Morherr, A.; Witt, S.; Chernenkaya, A.; Backer, J.-P.; Schonhense, G.; Bolte, M.; Krellner, C. Crystal growth of new charge-transfer salts based on π -conjugated donor molecules. *Phys. B* **2016**, *496*, 98–105.
78. Girlando, A.; Painelli, A.; Pecile, C. Molecular vibration analysis of ionicity and phase transition in TMPD-TCNQ (1:1) charge transfer complex. *Mol. Cryst. Liq. Cryst.* **1984**, *112*, 325–343.

79. Bechgaard, K.; Kistenmacher, T.J.; Bloch, A.N.; Cowan, D.O. The crystal and molecular structure of an organic conductor from 4,4',5,5'-Tetramethyl $\Delta^{2,2'}$ -bis-1,3-diselenole-7,7,8,8-Tetracyano-*p*-quinodimethane [TMTSF-TCNQ]. *Acta Crystallogr. B* **1977**, *33*, 417–422.
80. Kistenmacher, T.J.; Emge, T.J.; Bloch, A.N.; Cowan, D.O. Structure of the red, semiconducting form of 4,4',5,5'-Tetramethyl $\Delta^{2,2'}$ -bis-1,3-diselenole-7,7,8,8-Tetracyano-*p*-quinodimethane, TMTSF-TCNQ. *Acta Crystallogr. B* **1982**, *38*, 1193–1199.
81. Goetz, K.P.; Tsutsumi, J.; Pookpanratana, S.; Chen, J.; Corbin, N.S.; Behera, R.K.; Coropceanu, V.; Richter, C.A.; Hacker, C.A.; Hasegawa, T.; et al. Polymorphism in the 1:1 charge-transfer complex DBTTF-TCNQ and its effects on optical and electronic properties. *Adv. Electron. Mater.* **2016**, *2*, 1600203.
82. Girlando, A. Comment on Polymorphism in the 1:1 charge-transfer complex DBTTF-TCNQ and its effects on optical and electronic properties. *Adv. Electron. Mater.* **2017**, *3*, 1600437.
83. Lapidus, S.H.; Naik, A.; Wixtrom, A.; Massa, N.E.; Ta Phuoc, V.; del Campo, L.; Lebègue, S.; Ángyán, J.G.; Abdel-Fattah, T.; Pagola, S. The black polymorph of TTF-CA: TTF polymorphism and solvent effects in mechanochemical and vapor digestion syntheses, FT-IR, crystal packing, and electronic structure. *Cryst. Growth Des.* **2013**, *14*, 91–100.
84. Kistenmacher, T.J.; Phillips, T.E.; Cowan, D.O. The crystal structure of the 1:1 radical cation–radical anion salt of 2,2'-bis-1,3-dithiole (TTF) and 7,7,8,8-tetracyanoquinodimethane (TCNQ). *Acta Crystallogr. B* **1974**, *30*, 763–768.
85. Emge, T.J.; Wiygul, F.M.; Ferraris, J.P.; Kistenmacher, T.J. Crystal structure and Madelung energy for the charge-transfer complex tetrathiafulvalene-2,5-difluoro-7,7,8,8-tetracyanoquinodimethane. Observations on a dimerized segregated stack motif. *Mol. Cryst. Liq. Cryst.* **1981**, *78*, 295–310.
86. Wiygul, F.M.; Emge, T.J.; Kistenmacher, T.J. Elements of the crystal structure of a solvated 1:1 charge-transfer salt derived from tetrathiafulvalene (TTF) and tetrafluorotetracyano-*p*-quinodimethane (TCNQF4), TTF-TCNQF4. *Mol. Cryst. Liq. Cryst.* **1982**, *90*, 163–171.



© 2017 by the authors. Licensee MDPI, Basel, Switzerland. This article is an open access article distributed under the terms and conditions of the Creative Commons Attribution (CC BY) license (<http://creativecommons.org/licenses/by/4.0/>).